1521-0103/370/3/823–833$35.00
THE JOURNAL OF PHARMACOLOGY AND EXPERIMENTAL THERAPEUTICS

https://doi.org/10.1124/jpet.119.257345
J Pharmacol Exp Ther 370:823–833, September 2019

The Journal of PHARMACOLOGY And Experimental Therapeutics

Special Section on Drug Delivery Technologies

δ-Tocopherol Effect on Endocytosis and Its Combination with Enzyme Replacement Therapy for Lysosomal Disorders: A New Type of Drug Interaction?[S]

Rachel L. Manthe,[1] Jeffrey A. Rappaport,[1] Yan Long, Melani Solomon, Vinay Veluvolu, Michael Hildreth, Dencho Gugutkov, Juan Marugan, Wei Zheng, and Silvia Muro

Fischell Department of Bioengineering (R.L.M., J.A.R., V.V., M.H.) and Institute for Bioscience and Biotechnology Research (M.S., S.M.), University of Maryland, College Park, Maryland; National Center for Advancing Translational Sciences, National Institutes of Health, Bethesda, Maryland (Y.L., J.M., W.Z.); Institute for Bioengineering of Catalonia of the Barcelona Institute of Science and Technology, Barcelona, Spain (D.G., S.M.); and Institution of Catalonia for Research and Advanced Studies, Barcelona, Spain (S.M.)

Received February 11, 2019; accepted May 15, 2019

ABSTRACT

Induction of lysosomal exocytosis alleviates lysosomal storage of undigested metabolites in cell models of lysosomal disorders (LDs). However, whether this strategy affects other vesicular compartments, e.g., those involved in endocytosis, is unknown. This is important both to predict side effects and to use this strategy in combination with therapies that require endocytosis for intracellular delivery, such as lysosomal enzyme replacement therapy (ERT). We investigated this using δ-tocopherol as a model previously shown to induce lysosomal exocytosis and cell models of type A Niemann-Pick disease, a LD characterized by acid sphingomyelinase (ASM) deficiency and sphingomyelin storage. δ-Tocopherol and derivative CF3-T reduced net accumulation of fluid phase, ligands, and polymer particles via phagocytic, caveolae-, clathrin-, and cell adhesion molecule (CAM)-mediated pathways, yet the latter route was less affected due to receptor overexpression. In agreement, δ-tocopherol lowered uptake of recombinant ASM by deficient cells (known to occur via the clathrin pathway) and via targeting intercellular adhesion molecule-1 (associated to the CAM pathway). However, the net enzyme activity delivered and lysosomal storage attenuation were greater via the latter route. Data suggest stimulation of exocytosis by tocopherols is not specific of lysosomes and affects endocytic cargo. However, this effect was transient and became unnoticeable several hours after tocopherol removal. Therefore, induction of exocytosis in combination with therapies requiring endocytic uptake, such as ERT, may represent a new type of drug interaction, yet this strategy could be valuable if properly timed for minimal interference.

Introduction

Lysosomal diseases (LDs) are a group of 50 to 60 different monogenic disorders characterized by deficient lysosomal function (Futerman and van Meer, 2004). This is often caused by a defective lysosomal hydrolase, and, as a consequence, lysosomes accumulate respective undigested metabolites (Ballabio and Gieselmann, 2009). Because lysosomes are vital to many cellular functions, this aberrant storage leads to alterations in signaling pathways, cytoskeletal arrangement, autophagy, lipid trafficking, etc., manifesting into a wide array of life-threatening symptoms, including premature death (Simons and Gruenberg, 2000; Fukuda et al., 2006; Parkinson-Lawrence et al., 2010).

Currently, there are a number of clinical and experimental treatments for LDs, including therapies based on small molecules that act as chemical chaperones or inhibit

This work was supported by the National Institutes of Health [Grant R01 HL98416]; Spanish Ministry of Economy and Competitiveness—MINECO/FEDER Project SEV-2014-0425, Spanish Ministry of Science, Innovation and University—MINECO/EXPLORA Project SAF2017-91909-EXP and MINECO/RETOS Project RTI2018-101034-B-I00, and CERCA Program of the Generalitat de Catalunya (awarded to S.M.); National Science Foundation Graduate Research Fellowship [DGE-0750616], University of Maryland Flagship Fellowship, and the National Institutes of Health Ruth L. Kirschstein Predoctoral Fellowship [F31-HL128121 (awarded to R.L.M.)]; Howard Hughes Medical Institute Fellowship Program under the University of Maryland Undergraduate Science Education Program (awarded to J.A.R.); and Intramural Research Program of the National Institutes of Health National Center for Advancing Translational Sciences (awarded to W.Z.).
[1]R.L.M. and J.A.R. contributed equally to this work.
https://doi.org/10.1124/jpet.119.257345.
[S] This article has supplemental material available at jpet.aspetjournals.org.

ABBREVIATIONS: ASM, acid sphingomyelinase; CAM, cell adhesion molecule; CTB, cholera toxin subunit B; ERT, enzyme replacement therapy; FITC, fluorescein isothiocyanate; HEX, hexosaminidase; ICAM-1, intercellular adhesion molecule 1; LD, lysosomal disorder; NPC1, type C1 Niemann-Pick disease; NPD-A, type A Niemann-Pick disease; Tf, transferrin; TNFα, tumor necrosis factor α.

metabolite synthesis, gene therapy to produce functional enzyme activity, and i.v. infusion of recombinant enzymes to replace those that are deficient, known as enzyme replacement therapy (ERT) (Solomon and Muro, 2017). These approaches are highly valuable for individual diseases; however, they are specific to the genetic defect and/or lysosomal storage of each particular disease, for which they do not represent universal treatment options for LDs. An alternative or complementary approach recently proposed, which would be applicable to most LDs, is the induction of lysosomal exocytosis. This would enable cellular secretion of the metabolites stored in diseased lysosomes to the extracellular milieu, where they can be removed by the lymphatics, the immune system, etc. (Klein et al., 2005; Chen et al., 2010; Strauss et al., 2010; Medina et al., 2011; Xu et al., 2012; Spampanato et al., 2013; Cao et al., 2015; Long et al., 2016; Zhong et al., 2016).

Lysosomal exocytosis is a natural event (Schultz et al., 2011; Samie and Xu, 2014), and, in fact, secreted lysosomal substrates have been found in the urine of LD patients, validating this clearance mechanism as a potential treatment strategy (Whitley et al., 1989a,b; Wisniewski et al., 1994). Hence, this process can be capitalized for therapeutic purposes. Approaches to stimulate lysosomal exocytosis include the use of 2-hydroxypropyl-β-cyclodextrin in mouse-derived, type C1 Niemann-Pick (NPC1) cell models (Chen et al., 2010) and agonists of lysosomal big conductance calcium-activated Big Potassium (BK) channels in NPC1, mucolipidosis type IV, NPD-A, and Fabry disease (Cao et al., 2015; Zhong et al., 2016). Also, overexpression of transcription factor EB, a key regulator of lysosomal biogenesis and function, or that of one of its target proteins (TRPML1), enhances lysosomal exocytosis and alleviates storage in several LDs (Medina et al., 2011; Spampanato et al., 2013; Samie and Xu, 2014). Although less relevant translationally, this paradigm can be modeled in cell culture using the vitamin E species, δ-tocopherol (Xu et al., 2012; Long et al., 2016). Incubation of LD cells with this compound and some of its derivatives results in reduction in lysosome size, lysosome distribution closer to the plasma membrane, enhanced lysosomal enzyme activity in the extracellular medium, and significant attenuation of lysosomal storage, as shown for cell models of type C Niemann-Pick disease, type A Niemann-Pick disease (NPD-A), Wolman disease, and other LDs (Xu et al., 2012; Long et al., 2016).

Although lysosomal exocytosis holds interest as a potential treatment option for LDs, it is unclear whether induction of lysosomal exocytosis may also cause exocytosis of related vesicles, such as endocytic ones. This is critical for many cellular functions, such as uptake of nutrients, signal transduction, plasmalemma recycling, pathogen defense, etc. (Mellman, 1996; Conner and Schmid, 2003), and also for delivery of other therapeutics that require endocytic uptake for intracellular delivery (Muro, 2012a; Rappaport et al., 2016). This is particularly relevant for LDs because many of these diseases have been reported to associate with diminished endocytic activity via clathrin, caveolae, cell adhesion molecule (CAM), macropinocytosis, etc. (Liscum and Faust, 1987; Marks and Pagano, 2002; Dhami and Schuchman, 2004; Hortsch et al., 2010; Teixeira et al., 2014; Kuech et al., 2016; Rappaport et al., 2016). This affects uptake of bulk fluid phase, ligands of receptor-mediated pathways, recycling of membrane proteins and lipids, etc., as found for NPC1, NPD-A, Pompe, Fabry, and Gaucher diseases (Liscum and Faust, 1987; Marks and Pagano, 2002; Dhami and Schuchman, 2004; Hortsch et al., 2010; Kuech et al., 2016; Rappaport et al., 2016). Induction of exocytosis could affect endocytic vesicles that bring cargo into diseased cells, further lowering their uptake capacity. Because most of these pathways have been explored for drug delivery and lysosomal ERT (Muro et al., 2003, 2006b; Nichols, 2003; Hillaireau and Couvreur, 2009; Boado et al., 2011; Chrastina et al., 2011; McMahon and Boucrot, 2011; Duncan and Richardson, 2012; Muro, 2012b; Rappaport et al., 2016; Garnacho et al., 2017), collateral exocytosis of endocytic vesicles could also hinder treatment by means that require endocytic uptake, such as gene therapy or ERT.

In this work, we explored this question using the δ-tocopherol model of lysosomal exocytosis and cellular models of acid sphingomyelinase (ASM)-deficient NPD-A because of the following reasons: 1) this LD associates with endocytic alterations in various routes (Dhami and Schuchman, 2004; Rappaport et al., 2016); 2) several of these routes are being investigated for ERT delivery (Solomon and Muro, 2017); and 3) lysosomal exocytosis can be induced in NPD-A cells by δ-tocopherol (Xu et al., 2012). Our results described below shed light into the potential effects of inducing lysosomal exocytosis on endocytic uptake and implications for combination therapy with recombinant enzymes.

Materials and Methods

Antibodies and Reagents. δ-Tocopherol was from Sigma-Aldrich (St. Louis, MO). CF3-T was synthesized internally, as published (Marugan et al., 2014). Alexa Fluor 594-transferrin (Tf) and cholera toxin subunit B (CTB), Texas Red dextran (10,000 MW), BODIPY-FL-C_{12}-sphingomyelin, and Texas Red goat anti-mouse IgG were from Invitrogen (Carlsbad, CA). Lysenin and rabbit anti-lysenin serum were from Wako Chemicals (Richmond, VA). Nile Red, filipin, imipramine hydrochloride, and 4-methylumbelliferyl-N-acetyl-β-D-glucosaminide were from Sigma-Aldrich. Mouse monoclonal anti-human intercellular adhesion molecule 1 (ICAM-1) clone R6.5 (anti-ICAM) was purified from HB-9580 hybridoma (American Type Culture Collection, Manassas, VA). Rabbit polyclonal anti-early endosome antigen 1 (anti-EEA-1) was from Cell Signaling Technologies (Danvers, MA). Mouse IgG, fluorescein isothiocyanate (FITC) anti-rabbit IgG, and Alexa Fluor 488 mouse anti-rabbit IgG were from Jackson ImmunoResearch (West Grove, PA). Polystyrene beads were from Polysciences (Warrington, PA). Recombinant human ASM (He et al., 1999) was provided by E. Schuchman (Department of Genetics and Genomic Sciences, Mount Sinai School of Medicine, New York, NY) or commercially obtained from Abcam (Cambridge, UK). 6-Hexadecanoylamino-4-methylumbelliferyl-phosphorylcholine was from Moscerdam Substrates (Oegstgeest, The Netherlands). ^{125}Iodine (^{125}I) was from Perkin-Elmer (Waltham, MA), and Pierce iodination tubes were from Thermo Fisher Scientific (Waltham, MA). Unless otherwise noted, all other reagents were from Sigma-Aldrich.

Cell Cultures. Pharmacological models consisted of human umbilical vein endothelial cells (Lonza, Walkersville, MD) seeded on gelatin-coated coverslips and incubated at 37°C, 5% CO_2, and 95% relative humidity in M-199 medium (Invitrogen) supplemented with 15% FBS, 15 μg/ml endothelial cell growth supplement, 2 mM L-glutamine, 100 μg/ml heparin, and antibiotics. To mimic lysosomal storage characteristic of NPD-A, human umbilical vein endothelial cells were incubated for 4 days at 37°C with 20 μM imipramine, which degrades endogenous ASM (Hurwitz et al., 1994). Genetic models were primary, human skin fibroblasts from wild-type or NPD-A (GM13205 with deletion of a cytosine in codon 330) subjects from the Coriell Cell Repository (Camden, NJ) that were cultured in Dulbecco's modified

Eagle's medium (Gibco, Grand Island, NY) supplemented with 10% FBS, 2 mM L-glutamine, and antibiotics. Where indicated, cells were treated for 48 hours prior to assays with 40 μM δ-tocopherol or 20 μM CF3-T.

Preparation of Nano- and Microparticles. For studies on the CAM pathway and enzyme delivery, respectively, anti-ICAM alone (4.8 μM) or a 50:50 mass ratio of anti-ICAM:ASM (1.36 μM:2.72 μM) was coated by surface adsorption onto 100-nm–diameter, green Fluoresbrite polystyrene particles (anti-ICAM and anti-ICAM/ASM nanocarriers (NCs), respectively), as described (Serrano et al., 2016; Garnacho et al., 2017). Anti-ICAM NCs loaded with ASM at this ratio efficiently target the CAM route and deliver active ASM to lysosomes, leading to effective degradation of accumulated substrates in cells and mice (Muro et al., 2006b; Garnacho et al., 2008, 2017). The hydrodynamic diameter and polydispersity index of coated particles were measured by dynamic light scattering (Malvern Instruments, Westborough, MA) and found to be, respectively, 269 ± 4 nm and 0.17 ± 0.01 for anti-ICAM NCs, and 243 ± 2 nm and 0.15 ± 0.01 for anti-ICAM/ASM NCs. To characterize coating, anti-ICAM or ASM was conjugated to ^{125}I, and the amount of antibody or enzyme per particle was quantified using a γ counter (2470 Wizard^2; Perkin Elmer) and their respective specific activities (cpm/mass), as reported (Serrano et al., 2016; Garnacho et al., 2017). Anti-ICAM NCs contained 257 ± 9 anti-ICAM molecules per NC, and anti-ICAM/ASM NCs had 135 ± 5 anti-ICAM molecules and 259 ± 1 ASM molecules per NC, in accord with previous reports (Garnacho et al., 2008, 2017). In saline or serum-containing medium, these formulations exhibit no aggregation, minimal antibody, or enzyme release (≤10% release), and minimal coating with serum albumin (≤5%) (Hsu et al., 2011, 2012; Serrano et al., 2016). As demonstrated (Muro et al., 2006a; Garnacho et al., 2008, 2017), these model carriers are comparable to clinically-relevant biodegradable poly(lactic-co-glycolic acid) ones in regard to coating efficiency, in vivo targeting, and intracellular trafficking, validating this model.

For studies on phagocytosis, nonfluorescent 1-μm–diameter polystyrene particles were coated by adsorption with mouse IgG (1 μm IgG-coated microparticles), rendering final size of 1.15 ± 0.04 μm, polydispersity index of 0.38 ± 0.06, and total coating of 47,522 ± 6007 IgG molecules per particle.

Intracellular Lipid Storage. Lipid levels and the number of vesicular storage compartments were measured in control versus diseased cells, including pharmacological and genetic NPD-A cell models, prior or after 1- to 24-hour treatment with δ-tocopherol or derivative CF3-T. For sphingomyelin staining, cells were fixed with cold 2% paraformaldehyde, permeabilized with 0.1% Triton X-100, blocked with 2% bovine serum albumin–PBS, and immunostained with 0.5 μg/ml lysenin, followed by rabbit antilysenin serum and 4 μg/ml (green) FITC-labeled secondary antibody. Also, fixed cells were stained with 50 μg/ml (blue) filipin to label cholesterol, or with 100 ng/ml (red) Nile Red to generically label lipids. Samples were visualized by fluorescence microscopy using an Olympus IX81 microscope (Olympus, Center Valley, PA); 40× or 60× UPlanApo oil immersion objectives (Olympus); and blue, green, and red fluorescence filters (1160A-OMD, 3540B-OMF, 4040B-OMF; Semrock, Rochester, NY). Images were obtained with an ORCA-ER camera (Hamamatsu, Bridgewater, NJ) and SlideBook 4.2 software (Intelligent Imaging Innovations, Denver, CO) and analyzed using Image-Pro 6.3 (Media Cybernetics, Bethesda, MD). To quantify lysosomal sphingomyelin, cholesterol, and generic lipids, the mean fluorescence intensity in the perinuclear region (3 μm around the nucleus) was quantified with subtraction of the mean fluorescence intensity of the cell periphery, which was considered nonlysosomal (likely plasmalemma) background. Cells were also imaged by phase contrast, from which the number of dark-refringent intracellular (storage) compartments was quantified. These analyses were performed for individual cells to capture the intercellular variability of the population.

Sphingomyelin levels were also addressed in bulk for the entire cell population, either prior or after 4-hour treatment using 5 μg/ml naked recombinant ASM. For this, cells were preincubated overnight with 0.2 μg/ml BODIPY-FL-C_{12}-sphingomyelin, which fluoresces green (513 nm) at high concentrations (Luzio et al., 2007a,b). Cells were washed and fixed, and the nuclei stained with Hoechst 33342. Sphingomyelin fluorescence was analyzed using an InCell2200 imaging system (GE Healthcare Bio-Sciences, Pittsburgh, PA).

ASM Activity. Endogenous ASM activity was measured by incubating cells for 2 hours at 37°C with 20 μM 6-hexadecanoylamino-4-methylumbelliferyl-phosphorylcholine, a profluorescence ASM substrate in buffer containing 1% Triton X-100. The supernatant was measured in a fluorescence plate reader with excitation and emission wavelengths of 385 and 450 nm. ASM activity was assessed in a similar manner after 48-hour treatment with 40 μM δ-tocopherol and/or after 4-hour treatment with 2.3 μg/ml recombinant ASM.

Bulk Fluid-Phase Uptake. Control versus diseased cells were treated for 48 hours at 37°C with 40 μM δ-tocopherol or 20 μM CF3-T. Between 0 and 8 hours after removal of these agents, cells were incubated in fresh medium containing 1 mg/ml Texas Red dextran (a fluid-phase marker of endocytosis) for 1 hour at 37°C. Cells were then washed and fixed, and the number of fluorescent dextran-filled compartments per cell was analyzed by microscopy with an algorithm that quantifies fluorescent objects of 100- to 200-nm diameter with intensity above a background threshold level (Serrano et al., 2016).

Ligand and Particle Uptake. To evaluate the effect of δ-tocopherol on ligand uptake, healthy versus imipramine-induced diseased cells were treated for 48 hours at 37°C with 40 μM δ-tocopherol. Diseased cells that did not receive δ-tocopherol were used as control. Cells were then incubated between 1 and 3 hours at 37°C with one of the following agents: 20 μg/ml red Alexa Fluor594-labeled CTB (caveolae-mediated uptake), 50 μg/ml red Alexa Fluor594–labeled Tf (clathrin-mediated uptake), 7×10^{10} (green) Fluoresbrite anti-ICAM NCs/ml (CAM-mediated uptake), or 1×10^8 nonfluorescent 1 μm IgG-coated microparticles per milliliter (phagocytosis). Samples were then washed, fixed without permeabilization, and immunostained with secondary antibodies conjugated to green FITC or red Texas Red, opposite to the ligand or particle color. As previously demonstrated (Muro et al., 2003), this provides differential labeling of surface-located materials that are accessible for secondary staining versus internalized materials that are not accessible to said secondary staining (Muro et al., 2003). Thus, internalized materials appear as single-colored objects versus surface-bound materials, which appear as dual-colored objects (Muro et al., 2003). In the case of 1 μm IgG-coated microparticles, internalized microparticles lacked a fluorescent label, but these microparticles are visible and quantifiable from phase-contrast images, whereas surface-bound microparticles were immunolabeled in red. Where indicated, cells were treated with 10 ng/ml tumor necrosis factor α (TNFα) overnight prior to assay to mimic the inflammatory state found in NPD-A (Schuchman and Desnick, 2017).

Quantification of Early Endosomes. To discern whether δ-tocopherol may induce exocytosis of endosomal compartments, diseased cells were incubated at 37°C with 40 μM δ-tocopherol for either 15 minutes, 1 hour, or 3 hours. Thereafter, cells were fixed and permeabilized, and early endosomes were immunostained using anti–EEA-1 antibody, followed by washing and incubation with a secondary antibody labeled with green Alexa Fluor 488. Fluorescence microscopy images were taken and quantified using the settings and algorithm described above, to discern the number of ≥100-nm–diameter fluorescent objects with intensity level above the background level.

Lysosomal Secretion. To verify lysosome secretion, the release of the lysosomal enzyme β-hexosaminidase A and B (HEX) from the cell culture into the cell medium was examined. Control or diseased cells were treated for 24 hours at 37°C with 40 μM δ-tocopherol, and then this compound was removed and cells were incubated for up to 3 hours at 37°C with 10 μM ionomycin, an inducer of lysosome release, or 40 μM δ-tocopherol. The medium fraction was collected, and cells were washed, trypsinized, suspended in acidic buffer (10 mM monosodium phosphate, 5% glycerol buffer, pH 6.0), subjected to five freeze–thaw

cycles, and centrifuged at 16,000*g* for 20 minutes to pellet the insoluble membrane fraction, so that the soluble intracellular supernatant (cell fraction) was collected. Both the medium and cell fractions were incubated for 1 hour at 37°C in HEX substrate solution (2 mM 4-methylumbelliferyl-N-acetyl-β−D-glucosaminide, dissolved in 0.1 M citric acid/0.2 M disodium phosphate buffer, pH 4.5). Then the reaction was stopped with 0.4 M glycine–sodium hydroxide buffer (pH 10.4), and the fluorescent product was quantified in a plate reader (Spectramax M2; Molecular Devices) at λex = 360 nm and λem = 450 nm. The relative fluorescence units (RFU) were used to determine the percentage of HEX in each fraction using the following formula:

$$\%HEX\ in\ fraction = \frac{RFU(fraction) \times Volume\ of\ fraction}{(RFU(medium\ fraction) \times Volume\ of\ medium\ fraction) + (RFU(cell\ fraction) \times Volume\ of\ cell\ fraction)}$$

Uptake of Recombinant ASM. Diseased cells treated for 48 hours with 40 μM δ-tocopherol were incubated overnight with 10 ng/ml TNFα to mimic inflammation. The cells were then washed and incubated for 2 hours at 37°C with 2.1 μg/ml naked ^{125}I-ASM or a similar concentration of ^{125}I-ASM coupled to anti-ICAM NCs. Cells were washed to remove nonbound counterparts and incubated with an acid glycine solution (50 mM glycine and 100 mM NaCl at pH 2.5) to remove noninternalized ASM from the cell surface (Rappaport et al., 2015). The cells were then lysed in 2% Triton X-100, and the total ^{125}I-ASM present in the cell lysates was measured in a γ counter and corrected by subtraction of free ^{125}I, as determined by trichloroacetic acid precipitation.

Statistics. Data were calculated as the mean ± standard error of the mean (mean ± S.E.M.), where statistical significance for two-way comparisons was determined by Student's *t* test with a threshold of $P < 0.05$. Microscopy assays involved two to four experiments, each with at least two wells, from which 5 to 10 regions located throughout each sample, representative of the entire population, were selected for quantification. Each region contained a range of cells (4–10), all of which were individually analyzed. Fluorescence plate reader, enzyme activity, and radiotracing tests involved $n \geq 2$ independent experiment and $n \geq 3$ repeats per experiment.

Results

Effect of Tocopherols on Lysosomal Storage in NPD-A Cells. We first verified the effect of tocopherols on lysosomal exocytosis using vascular endothelial cells because they constitute one of the first cell linings encountered by i.v. injected therapies. As such, exocytosis induced in these cells could affect transport of recombinant enzymes to tissues. Because endothelial cells from NPD-A patients are unavailable, we first used a pharmacological model consisting of endothelial cells treated with imipramine (Muro et al., 2006b), whereas experiments described hereafter verify data in NPD-A patient fibroblasts. Imipramine enhances the degradation of endogenous ASM and mimics the intracellular lipid storage (sphingomyelin and cholesterol) characteristic of ASM-deficient NPD-A (Schuchman and Desnick, 2017). As expected, imipramine highly reduced endogenous ASM activity (87% reduction from control), similar to NPD-A patient fibroblasts (79% reduction from wild-type; Supplemental Fig. 1). Imipramine-induced diseased cells had enhanced intracellular storage of sphingomyelin (2.0-fold), cholesterol (3.5-fold), and overall lipids (2.3-fold) in perinuclear compartments, a location consistent with lysosomes, which drastically increased the total number of dark-refringent storage vesicles (22.4-fold) compared with control cells (Supplemental Fig. 2). This level of storage was comparable to NPD-A patient fibroblasts, which had 2.8-fold greater sphingomyelin and 3.8-fold greater cholesterol accumulation versus wild-type fibroblasts (Supplemental Fig. 3), validating this model.

Next, we examined whether the effect of tocopherols on lysosomal storage, which has been reported for patient fibroblasts and neural stem cells (Xu et al., 2012; Long et al., 2016), also applies to vascular endothelial cells. For this, imipramine-diseased endothelial cells were incubated for 48 hours with 40 μM δ-tocopherol or 20 μM analog CF3-T (Fig. 1A; Supplemental Fig. 4). As expected, both agents significantly decreased sphingomyelin storage by 33% and 48%, respectively, validating their effect on endothelial cells. In addition, treatment of imipramine-diseased endothelial cells with δ-tocopherol decreased the intracellular activity level of a control lysosomal enzyme HEX (20% reduction), whereas it increased the extracellular activity of this enzyme (30% increase; Fig. 1B), validating secretion of lysosomal content. This effect was almost equal to that of ionomycin, an agent known to induce lysosomal secretion, on control cells (Fig. 1B).

Effect of Tocopherols on Bulk Fluid-Phase Endocytosis. Having validated the imipramine-induced diseased cell model and tocopherol-induced reduction of storage, we focused on the effect of tocopherols on endocytic uptake. First, we tested nonspecific pinocytosis (bulk fluid-phase uptake), a process by which cells internalize extracellular fluid and

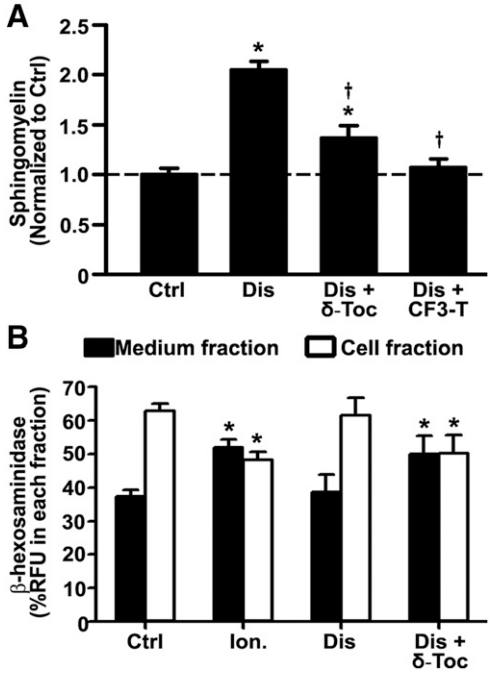

Fig. 1. Effect of tocopherols on sphingomyelin storage and lysosomal exocytosis in diseased endothelial cells. (A) Micrograph quantification of the perinuclear lysosomal staining of sphingomyelin using fluorescent lysenin, in control (Ctrl) vs. imipramine-diseased endothelial cells (Dis), prior or after 48-hour incubation with 40 μM δ-tocopherol (δ-Toc) or 20 μM CF3-T. Data are normalized to untreated control cells (horizontal dashed line). (B) Fluorimetric quantification of the enzymatic activity of lysosomal β-hexosaminidase in the cell medium (exocytosed) or the cell fraction (lysosomal) upon treatment of imipramine-diseased endothelial cells with δ-Toc, as in (A). Control endothelial cells treated or not with 10 μM ionomycin to cause lysosomal secretion are shown for a comparison (A and B). Data are mean ± S.E.M. ($n \geq 4$ independent wells). *Comparison with untreated control cells; †comparison with untreated diseased cells ($P < 0.05$ by Student's *t* test).

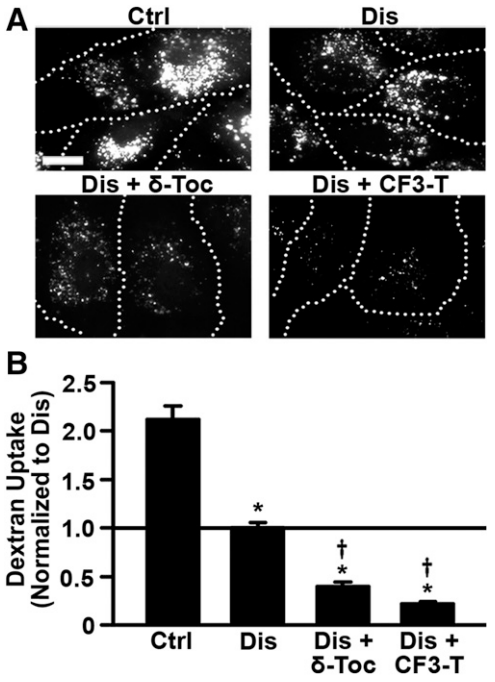

Fig. 2. Effect of tocopherols on bulk fluid-phase uptake in diseased endothelial cells. (A) Fluorescence microscopy of control (Ctrl) and imipramine-diseased endothelial cells (Dis) incubated for 1-hour pulse with Texas Red dextran, 1 hour after treating cells for 48 hours with 40 μM δ-tocopherol or 20 μM CF3-T. Dotted lines mark the cell borders, observed by phase-contrast microscopy. Scale bar, 10 μm. (B) Dextran uptake was quantified per cell and normalized to untreated diseased cells (horizontal solid line). Data are mean ± S.E.M. ($n \geq 4$ independent wells). *Comparison with untreated control cells; †comparison with untreated diseased cells ($P < 0.05$ by Student's t test).

solutes into endocytic vesicles. We used fluorescence microscopy to measure pinocytic uptake of the fluid-phase marker Texas Red dextran in imipramine-induced diseased endothelial cells treated with δ-tocopherol or CF3-T for 48 hours, then removed for 1 hour, versus diseased cells that lacked this treatment (Fig. 2A). As compared with control cells (Fig. 2B), dextran uptake was significantly reduced in diseased cells (53% reduction), which is consistent with published findings (Rappaport et al., 2015) on NPD-A patient fibroblasts (~40% reduction compared with wild-type), further validating this model. Importantly, bulk dextran endocytosis was further diminished in cells treated with δ-tocopherol or CF3-T (Fig. 2B), with CF3-T being a somewhat more potent inhibitor (61% and 78% reduction, respectively), in accord with its more potent effect on exocytosis (Fig. 1A). Reduced sphingomyelin storage was verified (26% and 41% reduction from untreated diseased cells, respectively; Supplemental Figs. 4 and 5), suggesting that induction of exocytosis by tocopherols alleviates lysosomal storage, but also lowers fluid-phase endocytosis.

Effect of δ-Tocopherol on Receptor-Mediated Endocytosis. Next, using fluorescently-labeled ligands, we examined the effect of δ-tocopherol on receptor-mediated endocytosis via caveoli (CTB), clathrin-coated pits (Tf), the CAM pathway [100 nm polymer nanocarriers targeted to ICAM-1; hereafter called anti-ICAM NCs (see *Materials and Methods* for characterization)], and phagocytosis (1 μm IgG-coated microparticles). Specificity of the uptake pathways for these ligands has been validated and can be found in our previous studies (Rappaport et al., 2014, 2015, 2016). Because the effects observed were similar for δ-tocopherol and CF3-T, we focused on the first compound as an example.

We recently reported decreased caveolar endocytosis of CTB, which binds to ganglioside GM1, and clathrin-mediated uptake of Tf, which binds to the Tf receptor, in NPD-A patient fibroblasts (Rappaport et al., 2014, 2015). Uptake of anti-ICAM NCs via the CAM pathway was also decreased in this disease (Serrano et al., 2012), although this route appeared more efficient than others (Rappaport et al., 2015, 2016). In this work, we found that imipramine-induced diseased endothelial cells also showed a similar pattern (14%, 58%, and 80% uptake of control cells for clathrin, caveolae, and CAM pathways, and 80% of control for phagocytosis; Fig. 3A), validating again this model. Importantly, δ-tocopherol treatment further reduced CTB, Tf, and microparticle uptake versus untreated diseased cells (35%, 39%, and 55% reduction, respectively; Fig. 3B). In contrast, anti-ICAM NC uptake via the CAM pathway was unaffected (92% of untreated diseased cells; Fig. 3B). Treatment of control endothelial cells with δ-tocopherol showed a similar trend, with clathrin-, caveoae-, and phagocytosis-, but not CAM-mediated uptake being decreased (Supplemental Fig. 6), suggesting that this effect is specific of δ-tocopherol, not imipramine, used to generate the disease phenotype. Similar experiments were repeated upon treatment of diseased cells with TNFα, a cytokine that stimulates an inflammatory phenotype, as observed in NPD-A and other LDs (Muro et al., 2006b; Schuchman and Desnick, 2017). Under TNFα activation, δ-tocopherol caused even more pronounced reduction of caveolar CTB uptake and phagocytic uptake of IgG-coated microparticles (58% and 71% reduction from untreated TNFα-activated diseased cells), whereas it had less of an effect (20% reduction) on clathrin-mediated Tf uptake, and it did not impact CAM uptake of anti-ICAM NCs (97% of untreated TNFα-activated diseased cells; Fig. 3C).

Based on this, it appeared δ-tocopherol lowered ligand uptake by all pathways except for CAM-mediated endocytosis. This was surprising because if tocopherol had caused this effect by inducing exocytosis of endocytic vesicles, the CAM pathway should also be affected. Hence, we investigated this in more detail. As expected, given that inflammatory conditions cause ICAM-1 overexpression (Muro et al., 2006a), TNFα increased binding of anti-ICAM NCs to diseased cells (2.44-fold increase; Supplemental Fig. 7). Unexpectedly, δ-tocopherol treatment further enhanced binding in TNFα-activated diseased cells (1.37-fold increase over untreated TNFα-activated diseased cells; Fig. 4A). However, the rate of NC uptake in TNFα-activated cells treated with δ-tocopherol, measured as the internalized fraction of all cell-associated NCs, was indeed reduced by 31% (Fig. 4A). Therefore, as for the other pathways, δ-tocopherol does diminish uptake via CAM-mediated endocytosis, but, because it also enhances binding to ICAM-1, absolute uptake via this pathway does not change. Increased anti-ICAM NC binding by δ-tocopherol treatment was not found for nonactivated diseased cells (104% of binding in untreated nonactivated diseased cells; Fig. 4A); hence, this effect may result from the combination of TNFα activation and δ-tocopherol.

Similarly, the effect of TNFα on the activity of each endocytic pathway was also assessed (Fig. 4B). As expected, absolute uptake via the CAM pathway was significantly increased under inflammation regardless of δ-tocopherol

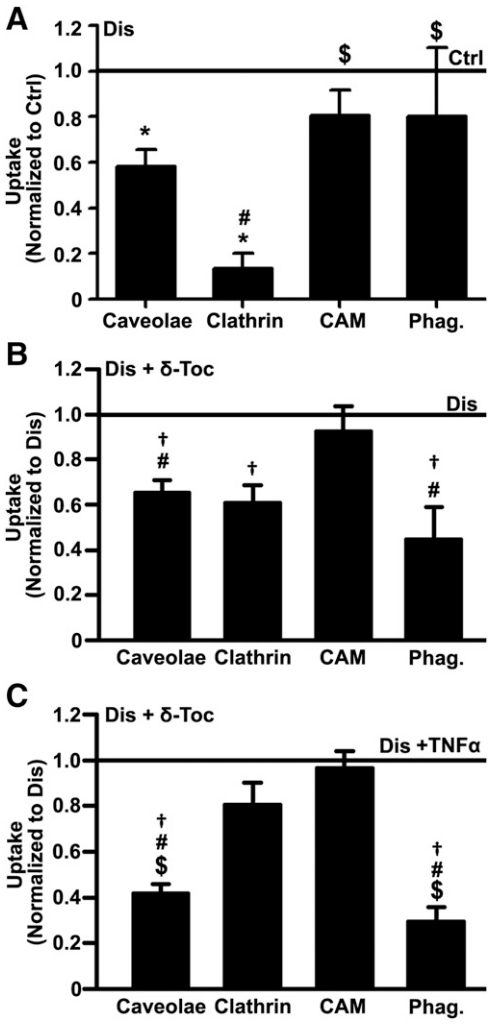

Fig. 3. Effect of δ-tocopherol on receptor-mediated uptake in diseased endothelial cells. (A) Microscopy quantification of the uptake (2-hour) of fluorescent ligands of individual endocytic pathways in imipramine-diseased endothelial cells (Dis) vs. control (Ctrl) cells. (B) Uptake of fluorescent ligands (3-hour) in imiprimine-diseased cells treated for 48 hours with 40 μM δ-tocopherol under noninflammatory or (C) inflammatory-like conditions (overnight incubation with TNFα). Ligands were CTB (caveolae-mediated endocytosis), Tf (clathrin-mediated endocytosis), 200 nm polymer nanocarriers targeted to ICAM-1 (anti-ICAM NCs; CAM-mediated endocytosis), and 1 μm IgG-coated microparticles (phagocytosis; Phag.). (A–C) After ligand incubation, cells were washed and fixed, and cell surface–bound ligands were immunostained with antibodies fluorescently labeled in a different color to distinguish internalized vs. surface-bound localization (see *Materials and Methods*). Data are mean ± S.E.M. ($n \geq 4$ independent wells), normalized to conditions shown in the horizontal solid lines. *Comparison with untreated diseased cells; †comparison with untreated diseased cells; #comparison with the CAM pathway; $comparison with the clathrin pathway ($P < 0.05$ by Student's t test).

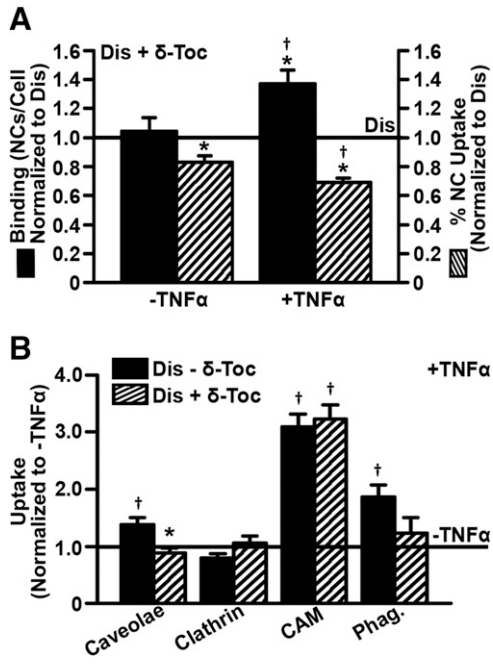

Fig. 4. δ-Tocopherol modulation of the TNFα effect on endocytosis in diseased endothelial cells. Imipramine-diseased endothelial cells (Dis) treated for 48 hours with 40 μM δ-tocopherol were left quiescent or activated overnight with TNFα to mimic inflammation. Cells were then incubated for 3 hours with (A) fluorescent anti-ICAM NCs or (B) fluorescent ligands of all individual endocytic pathways described in Fig. 3. Cells were washed and fixed, and cell surface ligands were fluorescently immunostained in a different color to distinguish internalized vs. surface-bound counterparts. (A) Binding was quantified as the total number of cell-associated fluorescent NCs, of which also the percentage of NCs internalized was measured. Data were normalized to untreated diseased cells (horizontal solid line). (B) Uptake of fluorescent ligands in TNFα-activated cells was normalized to nonactivated cells (horizontal solid line). (A and B) Data are mean ± S.E.M. ($n \geq 4$ independent wells). *Comparison with untreated diseased cells; †comparison with nonactivated cells ($P < 0.05$ by Student's t test).

treatment (~3-fold). Caveolae-mediated uptake of CTB and phagocytosis of IgG-coated microparticles by diseased cells were also increased by TNFα (1.4-fold and 1.9-fold, respectively), but δ-tocopherol inhibited this effect (0.9-fold and 1.2-fold of nonactivated diseased cells). Finally, clathrin-mediated uptake of Tf, which was lowered by δ-tocopherol (Fig. 3B), was not affected by TNFα (Fig. 4B).

Effect of δ-Tocopherol on Endosomal Compartments. Altogether, the data described to date indicate a generic effect of δ-tocopherol on the endocytic events. Because this vitamin has been shown to induce exocytosis of lysosomes (Xu et al., 2012; Long et al., 2016), which was verified in this study in Fig. 1B, we tested whether this was also the case for early endosomal compartments. As shown in Fig. 5A, treatment with δ-tocopherol decreased over time the visualization by fluorescence microscopy of EEA-1–positive vesicles, indicative of early endosomes, within the cell body of both imipramine-diseased endothelial cells and NPD-A fibroblasts. Image quantification (Fig. 5B) verified this: δ-tocopherol significantly reduced the number of EEA-1–positive compartments compared with controls (e.g., 29% and 34%, respectively, by 15-minute treatment).

Effect of δ-Tocopherol on Cell Uptake of Recombinant Enzymes Used for ERT. Given that tocopherols lowered endocytic content in diseased cells and the fact that ERT requires endocytic uptake of recombinant enzymes, we examined whether δ-tocopherol would affect delivery of recombinant ASM, the enzyme deficient in NPD-A (Schuchman and Desnick, 2017). As other enzymes used for lysosomal ERT, ASM undergoes clathrin-mediated endocytosis upon binding to M6P receptors (Dhami and Schuchman, 2004), which is blocked in the presence of competing M6P (Muro et al., 2006b). We first tested NPD-A patient fibroblasts to verify their lower level of endogenous ASM activity versus healthy cells (21% of control wild-type activity; Fig. 6A), and to verify that incubation with recombinant

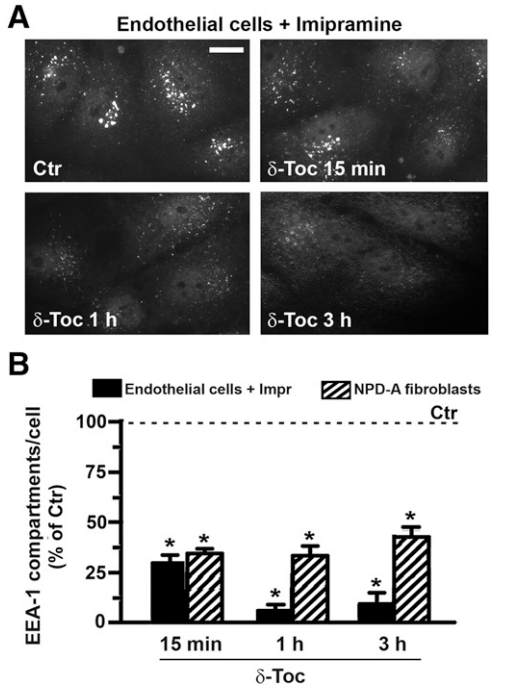

Fig. 5. δ-Tocopherol reduction of the number of EEA-1–positive compartments in diseased cells. Imipramine-diseased endothelial cells and NPD-A patient fibroblasts were left untreated (Ctr) or were treated with 40 μM δ-tocopherol for 15 minutes, 1 hour, or 3 hours. Cells were washed, fixed, and permeabilized, and early endosomes were labeled using anti–EEA-1, followed by secondary antibody conjugated to green Alexa Fluor 488. (A) Fluorescence microscopy images of endothelial cells, shown as an example. Scale bar, 10 μm. (B) Number of EEA-1–positive compartments per cell compared with absence of δ-tocopherol (Ctr), expressed as a percentage. Data are mean ± S.E.M. ($n \geq 4$ independent wells). *Comparison with Ctrl cells ($P < 0.05$ by Student's t test).

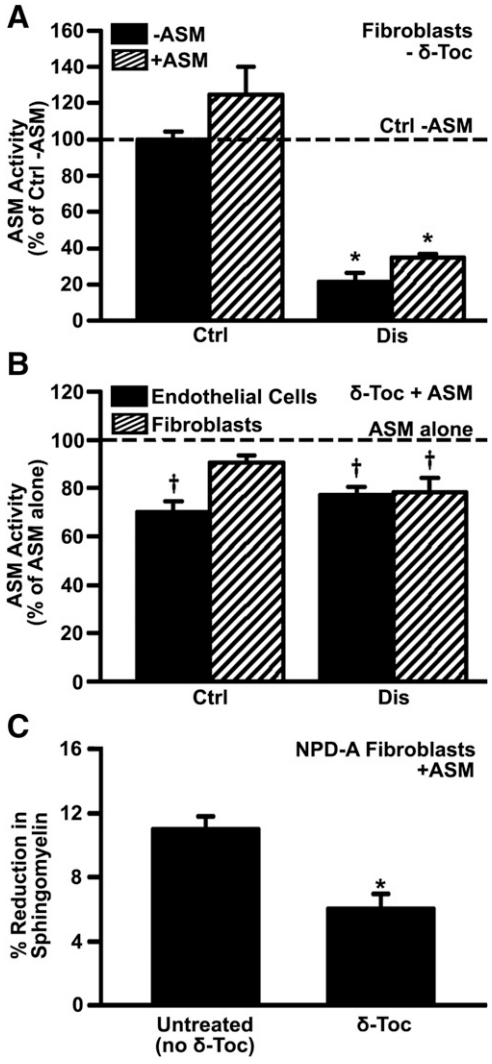

Fig. 6. Effect of δ-tocopherol on the activity provided by recombinant ASM to diseased cells. (A) ASM activity in wild-type (Ctrl) or NPD-A patient fibroblasts (Dis) incubated for 4 hours in the absence vs. presence of 2.3 μg/ml recombinant ASM. (B) ASM activity in healthy (Ctrl) vs. imipramine-diseased endothelial cells or NPD-A fibroblasts (Dis) after incubation for 4 hours with 2.3 μg/ml recombinant ASM, which was added after treatment with 40 μM δ-tocopherol. Data are normalized to (A) wild-type fibroblasts without ASM addition and to (B) untreated cells (respective horizontal dashed lines). (C) NPD-A fibroblasts treated for 48 hours with 40 μM δ-tocopherol and labeled with fluorescent sphingomyelin were washed and incubated with 5 μg/ml recombinant ASM for 4 hours, after which the sphingomyelin levels were measured in a plate reader. Data show sphingomyelin levels as a percentage of that found in cells not incubated with ASM. All data are mean ± S.E.M. ($n \geq 4$ independent wells). (A and B) *Comparison with wild-type fibroblasts without ASM addition; †comparison with untreated cells; (C) *comparison with untreated cells (all $P < 0.05$ by Student's t test).

ASM increased their ASM activity, as expected for delivery of an active enzyme (Fig. 6A). Recombinant ASM increased ASM activity of wild-type fibroblasts by 25% (not statistically significant due to high activity level in these cells) and to a greater extent (63% increase) in diseased cells, consistent with their lower endogenous activity. In contrast, treatment of cells (either endothelial cells or fibroblasts; Fig. 6B) with δ-tocopherol inhibited the acquisition of recombinant ASM activity by diseased cells (~22% reduction; Fig. 6B) and also lowered acquired ASM activity in healthy cells (9%–30% reduction; Fig. 6B). However, in the absence of recombinant ASM, δ-tocopherol did not affect endogenous ASM activity: 107% and 89% activity of untreated cells were found in imipramine-induced diseased endothelial cells or NPD-A fibroblasts, respectively (Supplemental Fig. 8). Thus, δ-tocopherol does not impact ASM activity per se, but diminishes acquisition of exogenous ASM activity, which is consistent with its effect in lowering the clathrin pathway, as was observed for Tf uptake (Fig. 3). As such, treatment with recombinant ASM was 45% less effective in reducing sphingomyelin storage in diseased cells treated with δ-tocopherol compared with those that did not receive this vitamin (Fig. 6C).

Then, because absolute uptake via the CAM pathway was relatively unaffected by δ-tocopherol, we tested uptake of recombinant ASM coupled to anti-ICAM NCs as an alternative approach (see *Materials and Methods* for NC characterization). Using ligand competition assays, this formulation has been verified to bind to ICAM-1, not M6PR, unlike naked ASM (Muro et al., 2006b). After 2 hours of incubation (Fig. 7A), total NC-mediated uptake of ASM (CAM pathway) was significantly enhanced versus uptake of naked ASM (clathrin route), both in the case of untreated diseased cells (48-fold enhancement by NCs) and δ-tocopherol–treated diseased cells (84-fold enhancement; Fig. 7A). As well, δ-tocopherol significantly reduced naked ASM uptake via the clathrin route (60% of untreated diseased cells; Fig. 7B), whereas the CAM pathway was unaffected (105% of untreated diseased cells), as expected based on previous experiments (Fig. 3).

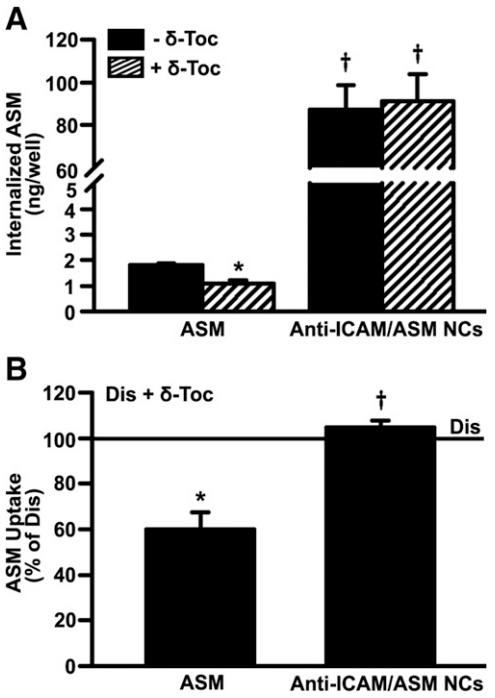

Fig. 7. Effect of δ-tocopherol on uptake of recombinant ASM via the clathrin vs. CAM pathways. Imipramine-diseased endothelial cells (Dis), activated overnight with TNFα and treated for 48 hours with 40 μM δ-tocopherol, were incubated for 2 hours with 2.1 μg/ml naked ^{125}I-ASM or ^{125}I-ASM coupled to anti-ICAM NCs (anti-ICAM/ASM NCs). After washing cells, an acid glycine solution was used to elute noninternalized ASM from the cell surface. ASM delivered into cells was then measured in the cell lysates. (A) Internalized ASM in cell lysates. (B) ASM uptake after treatment with δ-tocopherol as a percentage of untreated diseased cells (horizontal solid line). Data are mean ± S.E.M. ($n \geq 4$ independent wells). *Comparison with untreated diseased cells; †comparison with naked ASM ($P < 0.05$ by Student's t test).

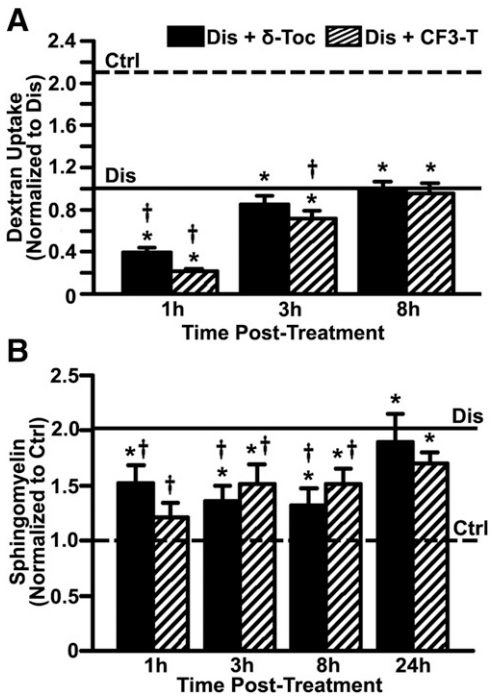

Fig. 8. Kinetics of tocopherol effect on bulk fluid-phase uptake and sphingomyelin levels. (A) Control (Ctrl) and imipramine-diseased endothelial cells (Dis) were incubated with Texas Red dextran (1 hour pulse) 1 to 8 hours after a 48-hour treatment with 40 μM δ-tocopherol or 20 μM CF3-T. Dextran uptake was normalized to untreated diseased cells (horizontal solid line). Dextran uptake by untreated control cells is shown by the horizontal dashed line. (B) Sphingomyelin was stained with fluorescent lysenin 1 to 24 hours after a 48-hour treatment with δ-tocopherol or CF3-T, quantified as described in Fig. 1, and normalized to untreated control cells (horizontal dashed line). Sphingomyelin levels in untreated diseased cells are shown by the horizontal solid line. Data are mean ± S.E.M. ($n \geq 4$ independent wells). *Comparison with untreated control cells; †comparison with untreated diseased cells ($P < 0.05$ by Student's t test).

Kinetics of the Tocopherol Effect on Lowering Endocytosis. Although we identified a pathway (CAM) less affected by tocopherols, the fact that δ-tocopherol lowered uptake of recombinant enzymes used for ERT suggests that combination treatment using both strategies may need optimal timing. To evaluate whether this effect is reversible, we examined the ability of cells to restore dextran pinocytosis upon removal of tocopherols because this marker showed good indication of uptake effects (Fig. 2). As shown in Fig. 8A, dextran uptake remained affected 3 hours after removal of δ-tocopherol or CF3-T from the cell medium (15% and 28% reduction vs. untreated diseased cells, respectively). Yet, 8 hours after removal, dextran uptake returned to the vitamin-untreated level in diseased cells (0.98-fold and 0.95-fold), suggesting that this effect is transient. During this 8-hour period, sphingomyelin storage in cells treated with δ-tocopherol or CF3-T remained below that in vitamin-untreated diseased cells (26% to 41% reduction; Fig. 8B). Hence, restoration of endocytosis seems due to cessation of tocopherol-induced exocytosis, not an increase in the sphingomyelin storage levels after tocopherol removal. As a control, sphingomyelin storage did not increase to diseased levels until 24 hours postremoval of δ-tocopherol or CF3-T (0.92-fold and 0.83-fold storage vs. vitamin-untreated diseased cells; Fig. 8B). Similar findings were obtained by quantifying the number of dark-refringent storage compartments by phase-contrast microscopy (Supplemental Fig. 9). Finally, a similar trend was observed for uptake of anti-ICAM NCs, whose binding and endocytosis recovered 5 hours after removal of δ-tocopherol (Supplemental Fig. 10), indicating this effect is reversible and combination therapy may be an option if properly timed.

Discussion

Lysosomal exocytosis is a constitutive event (Schultz et al., 2011; Samie and Xu, 2014) whose induction offers an avenue for LD treatment (Chen et al., 2010; Medina et al., 2011; Xu et al., 2012; Spampanato et al., 2013; Samie and Xu, 2014; Cao et al., 2015; Long et al., 2016; Zhong et al., 2016). Yet, the effect of this strategy on vesicles derived from endocytic pathways is unknown. Endosome–lysosome (like autophagosome–lysosome) fusion is a transient event, followed by lysosome reformation once substrate processing is complete (Luzio et al., 2007a,b; Fraldi et al., 2010). However, several LDs exhibit defects in intracellular trafficking, membrane fusion, and lysosome reformation, resulting in accumulation of early endosomes (Holroyd et al., 1999; Simons and Gruenberg, 2000; Fukuda et al., 2006; Yu et al., 2010; Andersen and Moestrup, 2014; Teixeira et al., 2014). Therefore, materials contained within endocytic vesicles may be expelled from the cell upon exocytosis induction, reducing

endocytic delivery of therapeutics, such as recombinant enzymes used for ERT. We evaluated this using tocopherols to induce lysosomal exocytosis. As suspected, this agent reduced endocytic uptake in NPD-A, the LD model studied, including dextran pinocytosis (Fig. 2) and receptor-mediated endocytosis of CTB, Tf, anti-ICAM NCs, and IgG-coated microparticles via caveolae-, clathrin-, CAM-, and phagocytosis-mediated mechanisms (Figs. 3 and 4), leading to decreased delivery and activity of a recombinant enzyme (Figs. 6 and 7).

This suggests that tocopherol-induced exocytosis affects endocytic vesicles and endosomes where separation of the ligand–receptor complex typically occurs prior to lysosomal trafficking (cargo) or recycling to the plasmalemma (receptor) (Mellman, 1996), lowering both cargo accumulation (Figs. 3 and 4) and number of EEA-1–positive early endosomes (Fig. 5). This would be possible if tocopherol-induced exocytosis operates through a mechanism common to different types of vesicles, which is supported by literature. For instance, endocytic recycling and vesicular trafficking along the endolysosomal route are calcium-dependent, just like lysosomal exocytosis (Knight, 2002; Luzio et al., 2007a,b; Lloyd-Evans et al., 2010; Yu et al., 2010; Cao et al., 2015). Additionally, tocopherols can undergo insertion in the membrane and alter its physical status (Ohyashiki et al., 1986; Bradford et al., 2003; Lemaire-Ewing et al., 2010). Because the expression and distribution of endocytic receptors, their adaptors, and/or signal transduction partners depend on the membrane physical properties, this could explain a generic effect of tocopherol on endocytosis regardless of the uptake route (Wells et al., 2010; Zingg, 2015). In fact, tocopherols can disrupt plasmalemma recruitment of protein kinase C, which is involved in all of the endocytic routes tested (Caron and Hall, 2001; Wells et al., 2010; Zingg, 2015).

Despite this generic effect, endocytosis was differently affected by δ-tocopherol for the caveolar-, clathrin-, phagocytic-, and CAM-mediated routes (Fig. 3). For the CAM pathway, the rate of anti-ICAM NC uptake was diminished by δ-tocopherol (Fig. 4A); yet, tocopherol enhanced NC binding to TNFα-activated cells (Fig. 4A), so that one effect balanced the other out (Fig. 3). Enhanced anti-ICAM NC binding by δ-tocopherol could be due to greater ICAM-1 expression or accessibility. If the first premise was true, binding to ICAM-1 should be greater upon δ-tocopherol treatment regardless whether or not cells were treated with TNFα; but this was not the case, ruling out this explanation. If tocopherol would have improved receptor access (Lemaire-Ewing et al., 2010; Wells et al., 2010), increased binding would also be expected regardless of TNFα, ruling out the second explanation. However, this could be explained if tocopherols induced generic exocytosis of intracellular vesicles: cells possess an intracellular pool of ICAM-1 in subplasmalemma vesicles that recycle back and forth the cell surface (Jo et al., 2010; Ghaffarian and Muro, 2014). The amount of ICAM-1 in these vesicles and the cell surface depends upon activation by cytokines such as TNFα (Descamps et al., 1997; Muro et al., 2003). Although tocopherols would not increase ICAM-1 expression (TNFα does), by enhancing exocytosis of intracellular ICAM-1, tocopherols would result in a greater membrane display of ICAM-1, supporting enhanced binding.

Similarly, δ-tocopherol reduced Tf uptake in TNFα-activated and nonactivated cells, although this effect was less acute in the former scenario (Fig. 3). Exocytosis and surface display of clathrin-associated receptors often sequestered in the Golgi–lysosome route in LDs (Dhami and Schuchman, 2004; Futerman and van Meer, 2004; Rappaport et al., 2014) would explain this. For the caveolar route, reduction of endocytic cargo by tocopherols could be due to several reasons. For instance, some tocopherol species (α-tocopherol) undergo membrane insertion predominantly into lipid rafts (Jiang et al., 2004; Royer et al., 2009), and treatment with γ- and δ-tocopherols interferes with sphingolipid synthesis (Jiang et al., 2004; Royer et al., 2009). Therefore, tocopherols may alter lipid raft formation and caveolae-mediated endocytosis, as observed (Fig. 3). Interestingly, TNFα increased caveolae-mediated uptake, in tune with previous reports (Wang et al., 2008; Chidlow and Sessa, 2010); yet, δ-tocopherol attenuated this effect (Fig. 4B).

For phagocytosis, impaired uptake of IgG-coated microparticles by δ-tocopherol seems counterintuitive because phagocytosis depends on endosome/lysosome exocytosis to recruit membrane at the cell surface for pseudopod extension (Champion and Mitragotri, 2006; Samie et al., 2013). Alterations in the membrane composition, structure, fluidity, etc., by δ-tocopherol may hinder large plasmalemma deformations. Although phagocytic uptake was improved by TNFα, consistent with literature (Nikolova and Russell, 1995), δ-tocopherol also reduced phagocytosis in the presence of this cytokine (Fig. 3).

Therefore, induction of lysosomal exocytosis as treatment of chronic diseases, such as LDs, may impact intracellular accumulation of endocytic cargo. Whether other exocytosis inductors lead to similar effects remains undetermined. This is important for the use of lysosomal exocytosis along with therapies needing intracellular delivery via endocytosis, such as ERT. For example, we observed reduced ASM activity delivered in cells treated with δ-tocopherol (Figs. 6 and 7), despite lack of an effect on endogenous ASM (Supplemental Fig. 8), indicating that tocopherols impact uptake of therapeutic enzymes. However, using lysosomal exocytosis to clear lysosomal storage first, followed by ERT, is an interesting alternative given that storage lowers uptake of recombinant enzymes (Dhami and Schuchman, 2004; Cardone et al., 2008; Rappaport et al., 2014). This is supported by the fact that reduced lysosomal storage was still observed 8 hours after δ-tocopherol removal (Fig. 8B; Supplemental Fig. 9), whereas endocytosis recovered between 5 and 8 hours (Fig. 8A; Supplemental Fig. 10). This duration is in relative agreement with observations on exocytosis induced by vitamin E derivatives (Xu et al., 2012) or by 2-hydroxypropyl-β-cyclodextrin (Chen et al., 2010; Liu et al., 2010). Said duration may depend on the cell type, lysosomal disease, agent employed to induce exocytosis, its concentration, in vivo pharmacokinetics, etc. As such, the timing for the use of agents inducing exocytosis along with agents requiring endocytosis must be investigated for each scenario.

Similarly, the effects of agents inducing exocytosis on the uptake of drug delivery systems may vary depending on the nanocarrier type, surface characteristics, targeting moieties, and drug cargo. For instance, the carrier composition, surface charge, stiffness, etc., can modulate cell interaction, uptake, and trafficking (Howard et al., 2014; Merkel et al., 2012; Muro, 2012a; Farokhirad et al., 2019). Yet, this varies for different targets: e.g., polystyrene, poly(lactic-co-glycolic acid), and

DNA-built nanocarriers targeting ICAM-1 showed relatively similar binding and uptake in cell culture and biodistribution in mice (Muro et al., 2006a; Muro, 2014; Garnacho et al., 2017). Also, the size of a drug carrier impacts its endocytic uptake, yet this effect depends on the mechanism of endocytosis: clathrin- and caveolae-mediated pathways are more severely affected by increasing the size of drug vehicles compared with CAM-mediated endocytosis (Champion and Mitragotri, 2006; Muro et al., 2008; Merkel et al., 2012; Howard et al., 2014). Carrier surface-to-volume ratio and angle of interaction with a cell also modulate uptake (Champion and Mitragotri, 2006), as well as the number of targeting moieties displayed on a nanocarrier (Serrano et al., 2016). Furthermore, the drug carried by a drug delivery vehicle can influence intracellular uptake and trafficking. For instance, ASM used in this work reduces NPD-A lysosomal storage (Garnacho et al., 2017). Because said lysosomal storage decreases uptake and endolysosomal trafficking in a "traffic jam" type of effect, by decreasing lysosomal storage, ASM also helps improve uptake and endolysosomal trafficking (Rappaport et al., 2016). Yet, other drugs without this property may be more severely affected by agents inducing exocytosis. In fact, many pharmaceutical agents impact negatively endocytosis and intracellular sorting, including drugs that alter the cytoskeleton, lysosomotropic compounds, and aminoglycoside antibiotics, which are used to fight certain cancers, infections, parasitoses, etc. (Muro, 2018). Therefore, it is expected that drug and nanocarrier parameters will further influence uptake efficacy in cells treated with δ-tocopherol or other agents causing exocytosis. Nevertheless, the fact that δ-tocopherol impacted uptake via all pathways examined even though very different cargoes were tested (a sugar polymer, proteins, and submicrometer- or micrometer-sized particles) suggests that any drug vehicle using endocytosis to access cells may be affected by agents that induce exocytosis.

Altogether, the results reported in this work will help guide future in vivo work to evaluate combination therapies for LDs using induction of lysosomal exocytosis and ERT, to minimize potential side effects and enhance treatment outcomes.

Acknowledgments

We thank Dr. Edward Schuchman (Department of Genetics and Genomic Sciences, Mount Sinai School of Medicine, New York, NY) for providing recombinant human ASM.

Authorship Contributions

Participated in research design: Muro, Marugan, Zheng.

Conducted experiments: Rappaport, Manthe, Long, Solomon, Hildreth, Veluvolu, Gugutkov.

Contributed new reagents or analytic tools: Marugan, Zheng.

Performed data analysis: Rappaport, Manthe, Long, Solomon, Hildreth, Veluvolu, Gugutkov, Zheng, Muro.

Wrote or contributed to the writing of the manuscript: Manthe, Rappaport, Solomon, Marugan, Zheng, Muro.

References

Andersen CB and Moestrup SK (2014) How calcium makes endocytic receptors attractive. *Trends Biochem Sci* **39**:82–90.

Ballabio A and Gieselmann V (2009) Lysosomal disorders: from storage to cellular damage. *Biochim Biophys Acta* **1793**:684–696.

Boado RJ, Hui EK, Lu JZ, Zhou QH, and Pardridge WM (2011) Reversal of lysosomal storage in brain of adult MPS-I mice with intravenous Trojan horse-iduronidase fusion protein. *Mol Pharm* **8**:1342–1350.

Bradford A, Atkinson J, Fuller N, and Rand RP (2003) The effect of vitamin E on the structure of membrane lipid assemblies. *J Lipid Res* **44**:1940–1945.

Cao Q, Zhong XZ, Zou Y, Zhang Z, Toro L, and Dong XP (2015) BK channels alleviate lysosomal storage diseases by providing positive feedback regulation of lysosomal Ca2+ release. *Dev Cell* **33**:427–441.

Cardone M, Porto C, Tarallo A, Vicinanza M, Rossi B, Polishchuk E, Donaudy F, Andria G, De Matteis MA, and Parenti G (2008) Abnormal mannose-6-phosphate receptor trafficking impairs recombinant alpha-glucosidase uptake in Pompe disease fibroblasts. *Pathogenetics* **1**:6.

Caron E and Hall A (2001) Phagocytosis, in *Endocytosis* (Marsh M ed) pp 58–77, Oxford University Press, Oxford, UK.

Champion JA and Mitragotri S (2006) Role of target geometry in phagocytosis. *Proc Natl Acad Sci USA* **103**:4930–4934.

Chen FW, Li C, and Ioannou YA (2010) Cyclodextrin induces calcium-dependent lysosomal exocytosis. *PLoS One* **5**:e15054.

Chidlow JH Jr and Sessa WC (2010) Caveolae, caveolins, and cavins: complex control of cellular signalling and inflammation. *Cardiovasc Res* **86**:219–225.

Chrastina A, Massey KA, and Schnitzer JE (2011) Overcoming in vivo barriers to targeted nanodelivery. *Wiley Interdiscip Rev Nanomed Nanobiotechnol* **3**:421–437.

Conner SD and Schmid SL (2003) Regulated portals of entry into the cell. *Nature* **422**: 37–44.

Descamps L, Cecchelli R, and Torpier G (1997) Effects of tumor necrosis factor on receptor-mediated endocytosis and barrier functions of bovine brain capillary endothelial cell monolayers. *J Neuroimmunol* **74**:173–184.

Dhami R and Schuchman EH (2004) Mannose 6-phosphate receptor-mediated uptake is defective in acid sphingomyelinase-deficient macrophages: implications for Niemann-Pick disease enzyme replacement therapy. *J Biol Chem* **279**:1526–1532.

Duncan R and Richardson SC (2012) Endocytosis and intracellular trafficking as gateways for nanomedicine delivery: opportunities and challenges. *Mol Pharm* **9**: 2380–2402.

Farokhirad S, Ranganathan A, Myerson J, Muzykantov VR, Ayyaswamy PS, Eckmann DM, and Radhakrishnan R (2019) Stiffness can mediate balance between hydrodynamic forces and avidity to impact the targeting of flexible polymeric nanoparticles in flow. *Nanoscale* **11**:6916–6928.

Fraldi A, Annunziata F, Lombardi A, Kaiser HJ, Medina DL, Spampanato C, Fedele AO, Polishchuk R, Sorrentino NC, Simons K, et al. (2010) Lysosomal fusion and SNARE function are impaired by cholesterol accumulation in lysosomal storage disorders. *EMBO J* **29**:3607–3620.

Fukuda T, Ewan L, Bauer M, Mattaliano RJ, Zaal K, Ralston E, Plotz PH, and Raben N (2006) Dysfunction of endocytic and autophagic pathways in a lysosomal storage disease. *Ann Neurol* **59**:700–708.

Futerman AH and van Meer G (2004) The cell biology of lysosomal storage disorders. *Nat Rev Mol Cell Biol* **5**:554–565.

Garnacho C, Dhami R, Simone E, Dziubla T, Leferovich J, Schuchman EH, Muzykantov V, and Muro S (2008) Delivery of acid sphingomyelinase in normal and Niemann-Pick disease mice using intercellular adhesion molecule-1-targeted polymer nanocarriers. *J Pharmacol Exp Ther* **325**:400–408.

Garnacho C, Dhami R, Solomon M, Schuchman EH, and Muro S (2017) Enhanced delivery and effects of acid sphingomyelinase by ICAM-1-targeted nanocarriers in type B Niemann-Pick disease mice. *Mol Ther* **25**:1686–1696.

Ghaffarian R and Muro S (2014) Distinct subcellular trafficking resulting from monomeric vs multimeric targeting to endothelial ICAM-1: implications for drug delivery. *Mol Pharm* **11**:4350–4362.

He X, Miranda SR, Xiong X, Dagan A, Gatt S, and Schuchman EH (1999) Characterization of human acid sphingomyelinase purified from the media of overexpressing Chinese hamster ovary cells. *Biochim Biophys Acta* **1432**:251–264.

Hillaireau H and Couvreur P (2009) Nanocarriers' entry into the cell: relevance to drug delivery. *Cell Mol Life Sci* **66**:2873–2896.

Holroyd C, Kistner U, Annaert W, and Jahn R (1999) Fusion of endosomes involved in synaptic vesicle recycling. *Mol Biol Cell* **10**:3035–3044.

Hortsch R, Lee E, Erathodiyil N, Hebbar S, Steinert S, Lee JY, Chua DS, and Kraut R (2010) Glycolipid trafficking in *Drosophila* undergoes pathway switching in response to aberrant cholesterol levels. *Mol Biol Cell* **21**:778–790.

Howard M, Zern BJ, Anselmo AC, Shuvaev VV, Mitragotri S, and Muzykantov V (2014) Vascular targeting of nanocarriers: perplexing aspects of the seemingly straightforward paradigm. *ACS Nano* **8**:4100–4132.

Hsu J, Northrup L, Bhowmick T, and Muro S (2012) Enhanced delivery of α-glucosidase for Pompe disease by ICAM-1-targeted nanocarriers: comparative performance of a strategy for three distinct lysosomal storage disorders. *Nanomedicine (Lond)* **8**:731–739.

Hsu J, Serrano D, Bhowmick T, Kumar K, Shen Y, Kuo YC, Garnacho C, and Muro S (2011) Enhanced endothelial delivery and biochemical effects of α-galactosidase by ICAM-1-targeted nanocarriers for Fabry disease. *J Control Release* **149**:323–331.

Hurwitz R, Ferlinz K, and Sandhoff K (1994) The tricyclic antidepressant desipramine causes proteolytic degradation of lysosomal sphingomyelinase in human fibroblasts. *Biol Chem Hoppe Seyler* **375**:447–450.

Jiang Q, Wong J, Fyrst H, Saba JD, and Ames BN (2004) gamma-Tocopherol or combinations of vitamin E forms induce cell death in human prostate cancer cells by interrupting sphingolipid synthesis. *Proc Natl Acad Sci USA* **101**:17825–17830.

Jo JH, Kwon MS, Choi HO, Oh HM, Kim HJ, and Jun CD (2010) Recycling and LFA-1-dependent trafficking of ICAM-1 to the immunological synapse. *J Cell Biochem* **111**:1125–1137.

Klein D, Büssow H, Fewou SN, and Gieselmann V (2005) Exocytosis of storage material in a lysosomal disorder. *Biochem Biophys Res Commun* **327**:663–667.

Knight DE (2002) Calcium-dependent transferrin receptor recycling in bovine chromaffin cells. *Traffic* **3**:298–307.

Kuech EM, Brogden G, and Naim HY (2016) Alterations in membrane trafficking and pathophysiological implications in lysosomal storage disorders. *Biochimie* **130**: 152–162.

Lemaire-Ewing S, Desrumaux C, Néel D, and Lagrost L (2010) Vitamin E transport, membrane incorporation and cell metabolism: is alpha-tocopherol in lipid rafts an oar in the lifeboat? *Mol Nutr Food Res* **54**:631–640.

Liscum L and Faust JR (1987) Low density lipoprotein (LDL)-mediated suppression of cholesterol synthesis and LDL uptake is defective in Niemann-Pick type C fibroblasts. *J Biol Chem* **262**:17002–17008.
Liu B, Ramirez CM, Miller AM, Repa JJ, Turley SD, and Dietschy JM (2010) Cyclodextrin overcomes the transport defect in nearly every organ of NPC1 mice leading to excretion of sequestered cholesterol as bile acid. *J Lipid Res* **51**: 933–944.
Lloyd-Evans E, Waller-Evans H, Peterneva K, and Platt FM (2010) Endolysosomal calcium regulation and disease. *Biochem Soc Trans* **38**:1458–1464.
Long Y, Xu M, Li R, Dai S, Beers J, Chen G, Soheilian F, Baxa U, Wang M, Marugan JJ, et al. (2016) Induced pluripotent stem cells for disease modeling and evaluation of therapeutics for Niemann-Pick disease type A. *Stem Cells Transl Med* **5**: 1644–1655.
Luzio JP, Bright NA, and Pryor PR (2007a) The role of calcium and other ions in sorting and delivery in the late endocytic pathway. *Biochem Soc Trans* **35**: 1088–1091.
Luzio JP, Pryor PR, and Bright NA (2007b) Lysosomes: fusion and function. *Nat Rev Mol Cell Biol* **8**:622–632.
Marks DL and Pagano RE (2002) Endocytosis and sorting of glycosphingolipids in sphingolipid storage disease. *Trends Cell Biol* **12**:605–613.
Marugan JJ, Zheng W, Xiao J, and McKew J (2014) inventors, National Institutes of Health assignee. Tocopherol and tocopheryl quinone derivatives as correctors of lysosomal storage disorders. U.S. patent 2014 WO/2014/078573.
McMahon HT and Boucrot E (2011) Molecular mechanism and physiological functions of clathrin-mediated endocytosis. *Nat Rev Mol Cell Biol* **12**:517–533.
Medina DL, Fraldi A, Bouche V, Annunziata F, Mansueto G, Spampanato C, Puri C, Pignata A, Martina JA, Sardiello M, et al. (2011) Transcriptional activation of lysosomal exocytosis promotes cellular clearance. *Dev Cell* **21**:421–430.
Mellman I (1996) Endocytosis and molecular sorting. *Annu Rev Cell Dev Biol* **12**: 575–625.
Merkel TJ, Chen K, Jones SW, Pandya AA, Tian S, Napier ME, Zamboni WE, and DeSimone JM (2012) The effect of particle size on the biodistribution of low-modulus hydrogel PRINT particles. *J Control Release* **162**:37–44.
Muro S (2012a) Challenges in design and characterization of ligand-targeted drug delivery systems. *J Control Release* **164**:125–137.
Muro S (2012b) Strategies for delivery of therapeutics into the central nervous system for treatment of lysosomal storage disorders. *Drug Deliv Transl Res* **2**: 169–186.
Muro S (2014) A DNA-device that mediates selective endosomal escape and intracellular delivery of drugs and biological. *Adv Funct Mater* **24**:2899–2906.
Muro S (2018) Alterations in cellular processes involving vesicular trafficking and implications in drug delivery. *Biomimetics* **3**:19.
Muro S, Dziubla T, Qiu W, Leferovich J, Cui X, Berk E, and Muzykantov VR (2006a) Endothelial targeting of high-affinity multivalent polymer nanocarriers directed to intercellular adhesion molecule 1. *J Pharmacol Exp Ther* **317**:1161–1169.
Muro S, Garnacho C, Champion JA, Leferovich J, Gajewski C, Schuchman EH, Mitragotri S, and Muzykantov VR (2008) Control of endothelial targeting and intracellular delivery of therapeutic enzymes by modulating the size and shape of ICAM-1-targeted carriers. *Mol Ther* **16**:1450–1458.
Muro S, Schuchman EH, and Muzykantov VR (2006b) Lysosomal enzyme delivery by ICAM-1-targeted nanocarriers bypassing glycosylation- and clathrin-dependent endocytosis. *Mol Ther* **13**:135–141.
Muro S, Wiewrodt R, Thomas A, Koniaris L, Albelda SM, Muzykantov VR, and Koval M (2003) A novel endocytic pathway induced by clustering endothelial ICAM-1 or PECAM-1. *J Cell Sci* **116**:1599–1609.
Nichols B (2003) Caveosomes and endocytosis of lipid rafts. *J Cell Sci* **116**:4707–4714.
Nikolova EB and Russell MW (1995) Dual function of human IgA antibodies: inhibition of phagocytosis in circulating neutrophils and enhancement of responses in IL-8-stimulated cells. *J Leukoc Biol* **57**:875–882.
Ohyashiki T, Ushiro H, and Mohri T (1986) Effects of alpha-tocopherol on the lipid peroxidation and fluidity of porcine intestinal brush-border membranes. *Biochim Biophys Acta* **858**:294–300.
Parkinson-Lawrence EJ, Shandala T, Prodoehl M, Plew R, Borlace GN, and Brooks DA (2010) Lysosomal storage disease: revealing lysosomal function and physiology. *Physiology (Bethesda)* **25**:102–115.
Rappaport J, Garnacho C, and Muro S (2014) Clathrin-mediated endocytosis is impaired in type A-B Niemann-Pick disease model cells and can be restored by ICAM-1-mediated enzyme replacement. *Mol Pharm* **11**:2887–2895.
Rappaport J, Manthe RL, Garnacho C, and Muro S (2015) Altered clathrin-independent endocytosis in type A Niemann-Pick disease cells and rescue by ICAM-1-targeted enzyme delivery. *Mol Pharm* **12**:1366–1376.
Rappaport J, Manthe RL, Solomon M, Garnacho C, and Muro S (2016) A comparative study on the alterations of endocytic pathways in multiple lysosomal storage disorders. *Mol Pharm* **13**:357–368.
Royer MC, Lemaire-Ewing S, Desrumaux C, Monier S, Pais de Barros JP, Athias A, Néel D, and Lagrost L (2009) 7-Ketocholesterol incorporation into sphingolipid/cholesterol-enriched (lipid raft) domains is impaired by vitamin E: a specific role for alpha-tocopherol with consequences on cell death. *J Biol Chem* **284**: 15826–15834.
Samie M, Wang X, Zhang X, Goschka A, Li X, Cheng X, Gregg E, Azar M, Zhuo Y, Garrity AG, et al. (2013) A TRP channel in the lysosome regulates large particle phagocytosis via focal exocytosis. *Dev Cell* **26**:511–524.
Samie MA and Xu H (2014) Lysosomal exocytosis and lipid storage disorders. *J Lipid Res* **55**:995–1009.
Schuchman EH and Desnick RJ (2017) Types A and B Niemann-Pick disease. *Mol Genet Metab* **120**:27–33.
Schultz ML, Tecedor L, Chang M, and Davidson BL (2011) Clarifying lysosomal storage diseases. *Trends Neurosci* **34**:401–410.
Serrano D, Bhowmick T, Chadha R, Garnacho C, and Muro S (2012) Intercellular adhesion molecule 1 engagement modulates sphingomyelinase and ceramide, supporting uptake of drug carriers by the vascular endothelium. *Arterioscler Thromb Vasc Biol* **32**:1178–1185.
Serrano D, Manthe RL, Paul E, Chadha R, and Muro S (2016) How carrier size and valency modulate receptor-mediated signaling: understanding the link between binding and endocytosis of ICAM-1-targeted carriers. *Biomacromolecules* **17**: 3127–3137.
Simons K and Gruenberg J (2000) Jamming the endosomal system: lipid rafts and lysosomal storage diseases. *Trends Cell Biol* **10**:459–462.
Solomon M and Muro S (2017) Lysosomal enzyme replacement therapies: historical development, clinical outcomes, and future perspectives. *Adv Drug Deliv Rev* **118**: 109–134.
Spampanato C, Feeney E, Li L, Cardone M, Lim JA, Annunziata F, Zare H, Polishchuk R, Puertollano R, Parenti G, et al. (2013) Transcription factor EB (TFEB) is a new therapeutic target for Pompe disease. *EMBO Mol Med* **5**:691–706.
Strauss K, Goebel C, Runz H, Möbius W, Weiss S, Feussner I, Simons M, and Schneider A (2010) Exosome secretion ameliorates lysosomal storage of cholesterol in Niemann-Pick type C disease. *J Biol Chem* **285**:26279–26288.
Teixeira CA, Miranda CO, Sousa VF, Santos TE, Malheiro AR, Solomon M, Maegawa GH, Brites P, and Sousa MM (2014) Early axonal loss accompanied by impaired endocytosis, abnormal axonal transport, and decreased microtubule stability occur in the model of Krabbe's disease. *Neurobiol Dis* **66**:92–103.
Wang L, Lim EJ, Toborek M, and Hennig B (2008) The role of fatty acids and caveolin-1 in tumor necrosis factor alpha-induced endothelial cell activation. *Metabolism* **57**:1328–1339.
Wells SR, Jennings MH, Rome C, Hadjivassiliou V, Papas KA, and Alexander JS (2010) Alpha-, gamma- and delta-tocopherols reduce inflammatory angiogenesis in human microvascular endothelial cells. *J Nutr Biochem* **21**:589–597.
Whitley CB, Draper KA, Dutton CM, Brown PA, Severson SL, and France LA (1989a) Diagnostic test for mucopolysaccharidosis. II. Rapid quantification of glycosaminoglycan in urine samples collected on a paper matrix. *Clin Chem* **35**:2074–2081.
Whitley CB, Ridnour MD, Draper KA, Dutton CM, and Neglia JP (1989b) Diagnostic test for mucopolysaccharidosis. I. Direct method for quantifying excessive urinary glycosaminoglycan excretion. *Clin Chem* **35**:374–379.
Wisniewski KE, Golabek AA, and Kida E (1994) Increased urine concentration of subunit c of mitochondrial ATP synthase in neuronal ceroid lipofuscinoses patients. *J Inherit Metab Dis* **17**:205–210.
Xu M, Liu K, Swaroop M, Porter FD, Sidhu R, Firnkes S, Ory DS, Marugan JJ, Xiao J, Southall N, et al. (2012) δ-Tocopherol reduces lipid accumulation in Niemann-Pick type C1 and Wolman cholesterol storage disorders [published correction appears in *J Biol Chem* (2013) 288:296]. *J Biol Chem* **287**:39349–39360.
Yu L, McPhee CK, Zheng L, Mardones GA, Rong Y, Peng J, Mi N, Zhao Y, Liu Z, Wan F, et al. (2010) Termination of autophagy and reformation of lysosomes regulated by mTOR. *Nature* **465**:942–946.
Zhong XZ, Sun X, Cao Q, Dong G, Schiffmann R, and Dong XP (2016) BK channel agonist represents a potential therapeutic approach for lysosomal storage diseases. *Sci Rep* **6**:33684.
Zingg JM (2015) Vitamin E: a role in signal transduction. *Annu Rev Nutr* **35**:135–173.

Address correspondence to: Dr. Silvia Muro, 5224 A. James Clark Hall, University of Maryland, Park, MD 20742. E-mail: muro@umd.edu

JPET# 257345

SUPPLEMENTAL DATA

δ-Tocopherol Effect on Endocytosis and its Combination with Enzyme Replacement Therapy for Lysosomal Disorders: a New Type of Drug Interaction?

*Rachel L. Manthe†, Jeffrey A. Rappaport†, Yan Long, Melani Solomon, Vinay Veluvolu, Michael Hildreth, Dencho Gugutkov, Juan Marugan, Wei Zheng, and Silvia Muro**

R.L.M., J.A.R., V.V. & M.H.: Fischell Department of Bioengineering, University of Maryland, College Park, MD 20742, USA

Y.L., J.M. & W.Z.: National Center for Advancing Translational Sciences, National Institutes of Health, Bethesda, MD 20892, USA

D.G. & S.M.: Institute for Bioengineering of Catalonia (IBEC) of the Barcelona Institute of Science and Technology (BIST), Barcelona, 02028, Spain

S.M.: Institution of Catalonia for Research and Advanced Studies (ICREA), Barcelona, 08010, Spain

M.S. & S.M.: Institute for Bioscience and Biotechnology Research, University of Maryland, College Park, MD 20742, USA

This work was supported by the National Institutes of Health [Grant R01 HL98416], Spanish Ministry of Economy and Competitiveness - MINECO/FEDER project SEV-2014-0425, Spanish Ministry of Science, Innovation and University - MINECO/EXPLORA project SAF2017-91909-EXP and MINECO/RETOS project RTI2018-101034-B-I00, and CERCA Program of the Generalitat de Catalunya awarded to S.M.; National Science Foundation Graduate Research Fellowship [DGE-0750616], University of Maryland Flagship Fellowship, the National Institutes of Health Ruth L. Kirschstein Pre-Doctoral Fellowship [F31-HL128121] awarded to R.L.M.; Howard Hughes Medical Institute Fellowship Program under the University of Maryland Undergraduate Science Education Program awarded to J.A.R.; and by Intramural Research Program of the National Institutes of Health [National Center for Advancing Translational Sciences] awarded to W.Z.

†These authors contributed equally to this article.

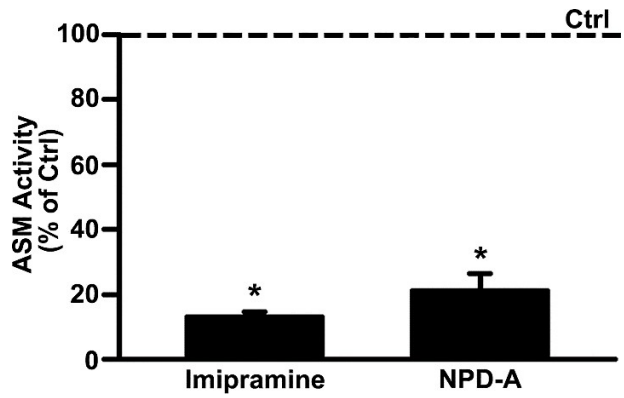

Figure S1. Endogenous ASM activity in pharmacological and genetic NPD-A cell models. ASM activity was determined in imipramine-diseased endothelial cells and NPD-A patient fibroblasts using an artificial substrate and measuring the resulting fluorescent product in a plate reader (see **Methods**). Data were normalized to control endothelial cells or wild-type fibroblasts, respectively (horizontal dashed line). Data are mean ± SEM (n≥4 independent wells). *Comparison to control cells ($p < 0.05$ by Student's *t*-test).

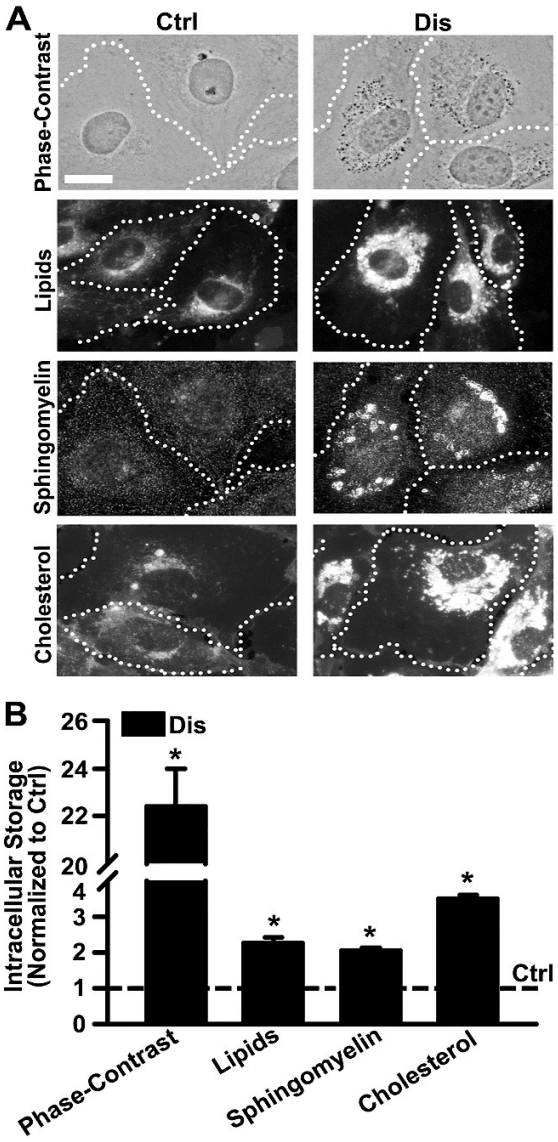

Figure S2. Induction of lipid storage in endothelial cells. (A) Microscopy of control (Ctrl) vs. imipramine-diseased endothelial cells (Dis). Dark-refringent storage compartments were visible by phase-contrast, and cells were additionally stained with fluorescent Nile Red to label lipids, lysenin to label sphingomyelin, or filipin to label cholesterol. Dotted lines mark the cell borders, as observed by phase-contrast. Scale bar = 10 µm. (B) The mean fluorescence intensity of markers in (A) was quantified within a 3 µm-perinuclear region, the background fluorescence (cell periphery) was subtracted, and data were normalized to control cells (horizontal dashed line). The number of dark-refringent storage compartments was quantified using phase-contrast images and also normalized to control cells. Data are mean ± SEM (n≥4 independent wells). *Comparison to control cells ($p < 0.05$ by Student's *t*-test).

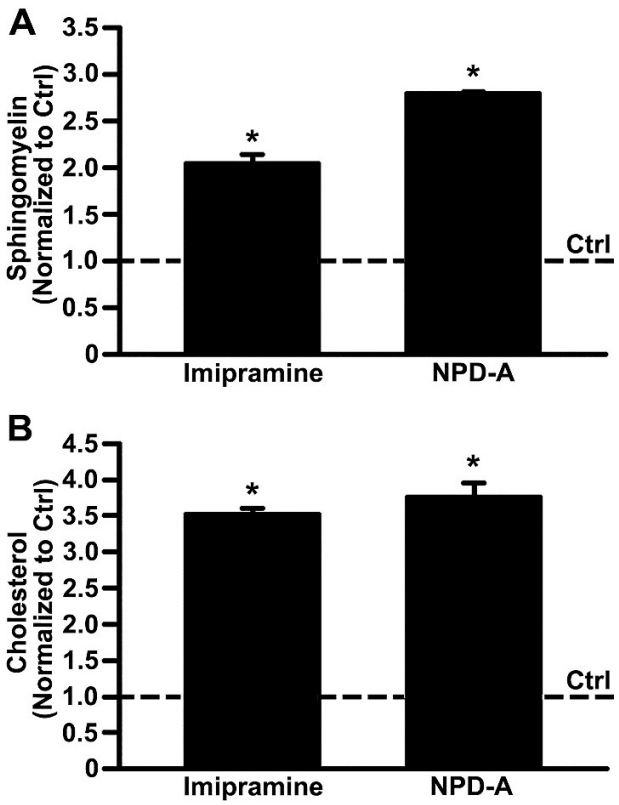

Figure S3. Sphingomyelin and cholesterol storage in pharmacological and genetic NPD-A cell models. Control and imipramine-diseased endothelial cells were stained with fluorescent lysenin or filipin to label sphingomyelin or cholesterol, respectively. Alternatively, sphingomyelin was labeled with fluorescent BODIPY-FL-C_{12}-sphinogmyelin in wild-type and NPD-A patient fibroblasts, and filipin was used to label cholesterol in these cells. The mean fluorescence intensity of (A) sphingomyelin and (B) cholesterol was quantified within a 3 μm-perinuclear region, the background fluorescence (cell periphery) was subtracted, and data were normalized to control cells (horizontal dashed line). Data are mean ± SEM (n≥4 independent wells). *Comparison to control cells ($p < 0.05$ by Student's *t*-test).

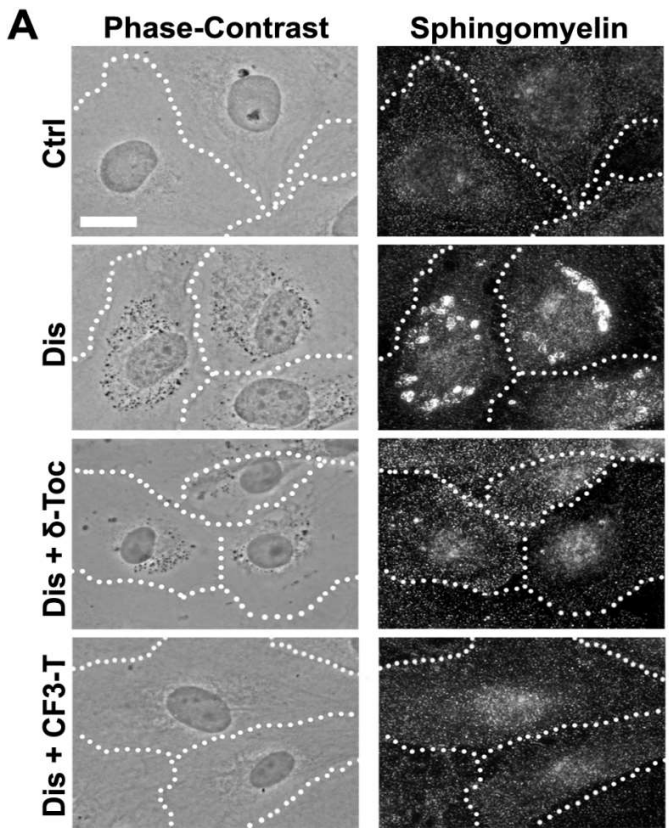

Figure S4. Micrographs of the effect of tocopherols on sphingomyelin storage in diseased endothelial cells. Phase-contrast and fluorescence microscopy images showing sphingomyelin accumulation (lysenin-positive) in control (Ctrl) vs. imipramine-diseased endothelial cells (Dis) after 48 h incubation in the absence or presence of 40 μM δ-tocopherol (δ-Toc) or 20 μM CF3-T. Dotted lines mark the cell borders, as observed by phase-contrast. Scale bar = 10 μm.

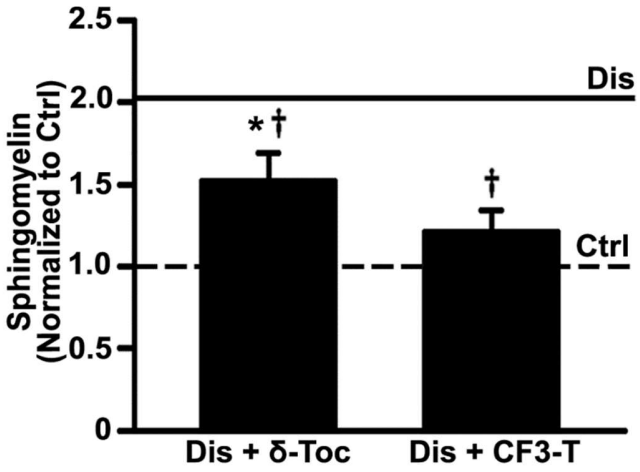

Figure S5. Reduction of sphingomyelin by tocopherols in diseased endothelial cells. Sphingomyelin was stained in imipramine-diseased endothelial cells (Dis) with fluorescent lysenin, 1 h after a 48 h treatment with 40 μM δ-tocopherol or 20 μM CF3-T. Sphingomyelin was then quantified as described in **Figure 1** and normalized to untreated control cells (horizontal dashed line) or untreated diseased cells (horizontal solid line). Data are mean ± SEM (n≥4 independent wells). *Comparison to untreated control cells; †comparison to untreated diseased cells indicated by the horizontal solid line ($p < 0.05$ by Student's *t*-test).

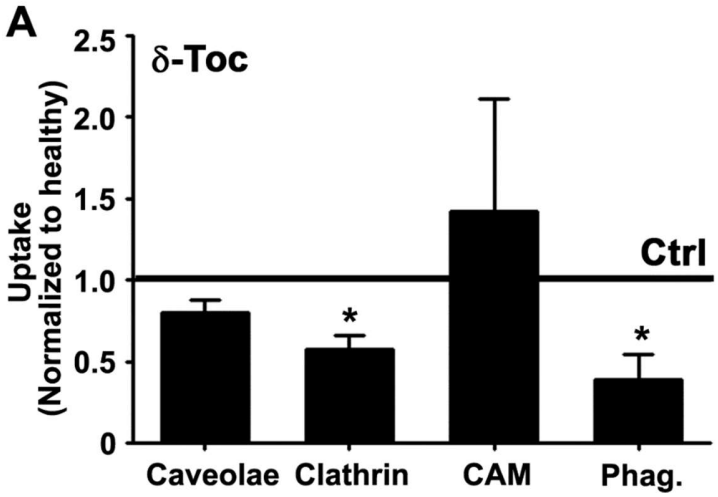

Figure S6. Effect of δ-tocopherol on receptor-mediated uptake in control endothelial cells. Control endothelial cells (Ctrl) were treated for 48 h with 40 μM δ-tocopherol, then incubated for 3 h with fluorescent ligands of individual endocytic pathways. Ligands were cholera toxin B (CTB; caveolae-mediated endocytosis), transferrin (Tf; clathrin-mediated endocytosis), 100 nm polymer nanocarriers targeted to ICAM-1 (anti-ICAM NCs; CAM-mediated endocytosis), and 1 μm IgG-coated microparticles (phagocytosis; Phag.). Thereafter, cells were washed, fixed, and cell-surface bound counterparts were immunostained with antibodies fluorescently-labeled in a different color to distinguish internalized vs. surface-bound ligands (see **Methods**). Uptake data are normalized to control cells (horizontal solid line). Data are mean ± SEM (n≥4 independent wells). *Comparison to control cells ($p < 0.05$ by Student's *t*-test).

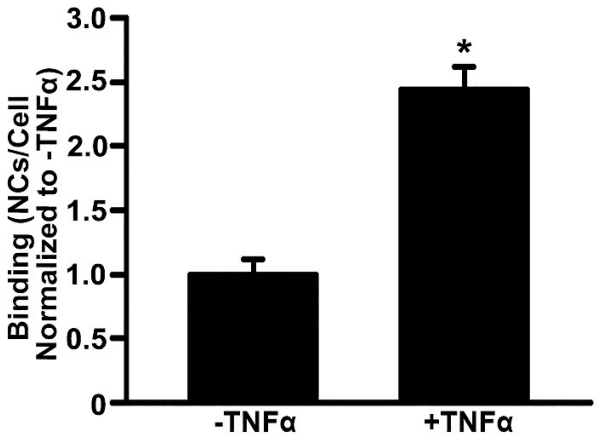

Figure S7. Effect of TNFα on anti-ICAM NC binding to diseased endothelial cells. Imipramine-diseased endothelial cells (Dis) were incubated overnight with control medium (-TNFα) or medium containing TNFα. Then, cells were incubated for 3 h with fluorescent anti-ICAM NCs, washed, fixed, and imaged by microscopy as described in **Figure 3**. Binding data are the fluorescent area of total cell-associated NCs normalized to control medium (-TNFα). Data are mean ± SEM (n≥4 independent wells). *Comparison to -TNFα cells ($p < 0.05$ by Student's *t*-test).

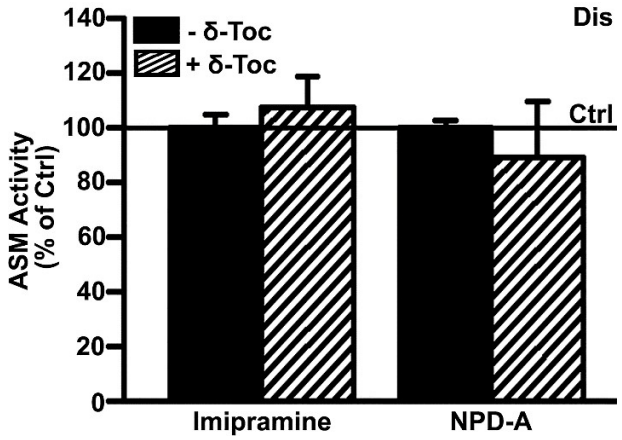

Figure S8. Effect of δ-tocopherol on endogenous ASM activity in pharmacological and genetic NPD-A cell models. The activity of endogenous ASM was measured in imipramine-diseased endothelial cells or NPD-A fibroblasts treated for 48 h with 40 μM δ-tocopherol as described in **Figure 6**. Data are normalized to untreated diseased endothelial cells or NPD-A fibroblasts (horizontal solid line). Data are mean ± SEM (n≥4 independent wells). No statistical significance was found.

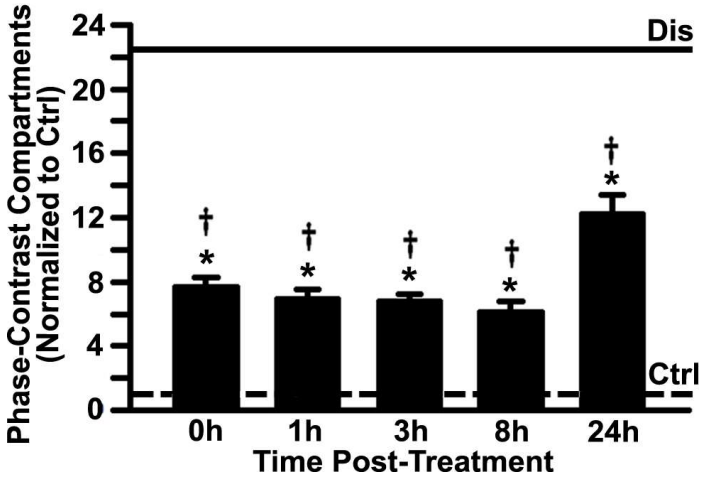

Figure S9. Effect of δ-tocopherol on dark-refringent storage compartments in diseased endothelial cells. Control (Ctrl) and imipramine-diseased endothelial cells (Dis) were incubated in fresh medium for 1-24 h after removal of 40 μM δ-tocopherol. Cells were washed, fixed, and the number of dark-refringent storage compartments was visualized by phase-contrast, quantified as described in **Figure S2**, and normalized to control cells (horizontal dashed line). Untreated diseased cells are shown as a horizontal solid line. Data are mean ± SEM (n≥4 independent wells). *Comparison to untreated control cells; †comparison to untreated diseased cells ($p < 0.05$ by Student's *t*-test).

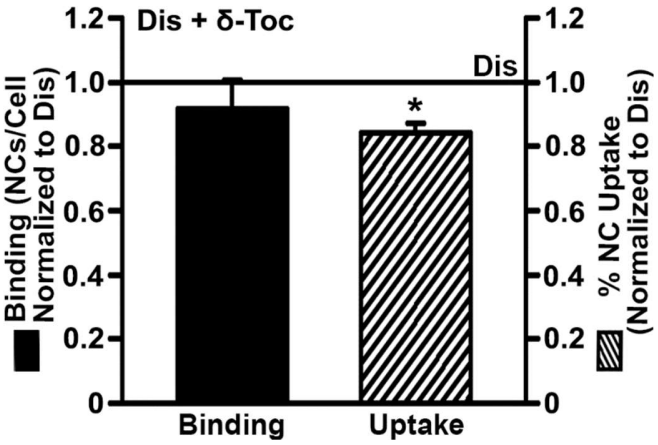

Figure S10. Anti-ICAM NC binding and uptake in diseased endothelial cells after δ-tocopherol removal. Imipramine-diseased endothelial cells (Dis) treated for 48 h with 40 μM δ-tocopherol were activated overnight with TNFα to mimic inflammation. Cells were then incubated for 3 h with fluorescent anti-ICAM NCs 5 h after removal of δ-tocopherol. Cells were washed, fixed, immunostained, and imaged by microscopy as described in **Figure 3**. Binding was quantified as total cell-associated fluorescent NCs, while NC uptake represents internalized NCs expressed as a percentage of the total cell-associated NCs. Data were normalized to untreated diseased cells (horizontal solid line). Data are mean ± SEM (n≥4 independent wells). *Comparison to untreated diseased cells ($p < 0.05$ by Student's *t*-test).